Liprin-α/SYD-2 determines the size of dense projections in presynaptic active zones in *C. elegans*

Maike Kittelmann,[1,2] Jan Hegermann,[1,3,4] Alexandr Goncharov,[5] Hidenori Taru,[5,7] Mark H. Ellisman,[6] Janet E. Richmond,[8] Yishi Jin,[5] and Stefan Eimer[1,3,9]

[1]European Neuroscience Institute, 37077 Göttingen, Germany
[2]Cellular Neurobiology, Schwann-Schleiden-Centre for Molecular Cell Biology, 37077 Göttingen, Germany
[3]Center for Molecular Physiology of the Brain, 37073 Göttingen, Germany
[4]Institute of Functional and Applied Anatomy, Hannover Medical School, 30625 Hannover, Germany
[5]Howard Hughes Medical Institute, Division of Biological Sciences; and [6]Center for Research on Biological Systems, National Center for Microscopy and Imaging Research and Department of Neurosciences; University of California, San Diego, La Jolla, CA 92093
[7]Laboratory of Neuronal Cell Biology, Graduate School of Pharmaceutical Sciences and Creative Research Institute, Hokkaido University, Kita-ku, Sapporo 060-0812, Japan
[8]Department of Biological Sciences, University of Illinois at Chicago, Chicago, IL 60607
[9]BIOSS Centre for Biological Signalling Studies, University of Freiburg, 79108 Freiburg, Germany

Synaptic vesicle (SV) release is spatially and temporally regulated by a network of proteins that form the presynaptic active zone (AZ). The hallmark of most AZs is an electron-dense projection (DP) surrounded by SVs. Despite their importance for our understanding of triggered SV release, high-resolution analyses of DP structures are limited. Using electron microscopy, we show that DPs at *Caenorhabditis elegans* neuromuscular junctions (NMJs) were highly structured, composed of building units forming bays in which SVs are docked to the AZ membrane. Furthermore, larger ribbonlike DPs that were multimers of the NMJ building unit are found at synapses between inter- and motoneurons. We also demonstrate that DP size is determined by the activity of the AZ protein SYD-2/Liprin-α. Whereas loss of *syd-2* function led to smaller DPs, *syd-2* gain-of-function mutants displayed larger ribbonlike DPs through increased recruitment of ELKS-1/ELKS. Therefore, our data suggest that a main role of SYD-2/Liprin-α in synaptogenesis is to regulate the polymerization of DPs.

Introduction

Fast synaptic neurotransmission relies on the triggered release of neurotransmitters from synaptic vesicles (SVs) after fusion with the plasma membrane. In axons, SVs are concentrated and exocytosed at active zones (AZs) of presynaptic terminals. To allow efficient communication within the neuronal network, SV release is a highly regulated process of sequential events (Sudhof, 2004; Richmond, 2005; Wojcik and Brose, 2007). SVs are first recruited to the AZ and then docked to the plasma membrane in a release competent state. This guarantees their rapid release after depolarization induced calcium influx into the presynaptic terminal. Recruitment, release, and subsequent endocytosis of SVs at the AZ are organized by an elaborate network of

proteins forming a complex cytomatrix (Dresbach et al., 2001; Schoch and Gundelfinger, 2006). However, despite its importance for orchestrating SV release, little is known about the ultrastructure of the AZ cytomatrix.

Classical analysis of AZ structures by EM revealed the existence of an electron-dense protein matrix called the dense projection (DP) at the center of AZs (Phillips et al., 2001; Zhai and Bellen, 2004). Depending on the organism and synapse type, DPs differ in size and structure, probably reflecting their different functional requirements. In central nervous system synapses of higher vertebrates, DPs have been shown to form a weblike grid of cone-shaped densities with intermediate slots for SV docking and fusion (Phillips et al., 2001). On the other hand, EM tomography of the frog neuromuscular junction (NMJ) revealed an elongated ribbonlike array that runs along the midline of the

Supplemental Material can be found at:
http://jcb.rupress.org/content/suppl/2013/12/04/jcb.201302022.DC1.html

The Rockefeller University Press $30.00
J. Cell Biol. Vol. 203 No. 5   849–863
www.jcb.org/cgi/doi/10.1083/jcb.201302022

JCB   849

presynaptic ridge with riblike tethers connecting SVs to the DP (Harlow et al., 2001). *Drosophila melanogaster* NMJs are characterized by DPs shaped like a T bar (Prokop and Meinertzhagen, 2006). In contrast, sensory ribbon synapses of the vertebrate ear or eye display a compact and spherical organization extending ≥1 µm into the cytoplasm of the presynaptic terminal (Zanazzi and Matthews, 2009; Regus-Leidig and Brandstätter, 2012). These large DPs recruit a characteristic halo of SVs, which are required for graded and sustained release at sensory synapses.

Only a few proteins are known to be directly involved in the organization and assembly of presynaptic DPs. In *Drosophila*, the long coiled-coil protein Bruchpilot (BRP) has been identified as a structural element of the T-bar DPs at NMJs (Kittel et al., 2006; Wagh et al., 2006; Fouquet et al., 2009). BRP was suggested to bring SVs in close proximity to voltage-gated calcium channels, augmenting sustained release. Loss of BRP leads to the disappearance of the T-bar AZ structures at NMJs (Kittel et al., 2006). In *Caenorhabditis elegans*, the multidomain protein SYD-2/Liprin-α has been shown to be involved in presynaptic AZ development (Zhen and Jin, 1999; Dai et al., 2006; Patel et al., 2006). Liprin-α was originally identified as an interaction partner of the receptor protein tyrosine phosphatase LAR (leukocyte common antigen related; Serra-Pagès et al., 1998). Its N-terminal coiled-coil domains and C-terminal sterile α motif domains mediate multiple interactions with a variety of synaptic proteins as well as the motor protein KIF1A/UNC-104 (Shin et al., 2003; Spangler and Hoogenraad, 2007; Wagner et al., 2009), suggesting a key role in AZ assembly. By recruiting synaptic components to specific presynaptic sites, SYD-2/Liprin-α serves as a scaffolding molecule organizing the formation of functional SV release machinery. Additionally, Liprin-α proteins exhibit strong homomeric interactions (Serra-Pagès et al., 1998), and a recent biochemical study implicates one of the two highly conserved N-terminal Liprin homology domains in the dimerization process and regulation of Liprin-α/SYD-2 clustering (Taru and Jin, 2011). Studies of *Drosophila* and mammalian Liprin-α also support its role in synapse development (Kaufmann et al., 2002; Wyszynski et al., 2002).

Loss-of-function (lof) mutations in *syd-2* were initially shown to form longer DPs in motoneuron synapses in *C. elegans* (Zhen and Jin, 1999). The same *syd-2* lof mutations cause impaired localization of most AZ proteins as well as SVs to synaptic sites in another synapse, the hermaphrodite-specific neuron (HSN; Patel et al., 2006). In addition, SV docking and synaptic transmission is impaired in *syd-2* lof mutants (Stigloher et al., 2011). Furthermore, a *syd-2* gain-of-function (gof) mutation is able to bypass the requirement of the SYD-2 upstream activator SYD-1. The ability of *syd-2* gof to promote AZ assembly requires the presence of the presynaptic AZ protein ELKS-1 (Dai et al., 2006). ELKS-1 and its homologues have been shown to localize to the AZ by immunohistochemistry and immuno-EM (Ohtsuka et al., 2002; Weimer et al., 2006) and interact with a variety of other AZ proteins, such as RIM1, Munc13-1 (Ohtsuka et al., 2002; Wang et al., 2002), Bassoon, Piccolo (Takao-Rikitsu et al., 2004), and SYD-2/Liprin-α (Ko et al., 2003). The N terminus of the *Drosophila* AZ protein BRP is partially homologous to human ELKS and *C. elegans* ELKS-1 (Wagh et al., 2006).

To understand the role of SYD-2 in AZ assembly, we have resolved the ultrastructure of AZ DPs using high-pressure freezing (HPF) cryofixation and serial EM reconstruction and EM tomography. Our analysis revealed a previously unknown basic ultrastructural unit for DPs in inter- and motoneuron synapses. We provide evidence that *syd-2* activity levels specifically control DP size. In addition, we show that the regulation of DP size mediated by SYD-2 is dependent on ELKS-1.

Results

3D reconstructions reveal the complex structure of presynaptic DPs

EM reconstructions from ultrathin (40 nm) serial cross sections of the nerve cords provided an initial assessment of NMJ DP morphology in motoneuron synapses (Fig. 1, A and B). The AZ DP was surrounded by a cluster of SVs, whereas the few dense core vesicles (DCVs) were localized in the periphery of the SV cluster (Fig. 1, B and C). The NMJ DPs were typically elongated along the axon and exhibited fibrous extensions emanating from this core structure to contact adjacent SVs (Fig. 1, A, D, and E). To overcome the limited resolution of the DP architecture in the z axis, we generated longitudinal ultrathin sections parallel to the length of the nerve cord and the AZ membrane. With such a top view onto the DPs, these sections revealed that the NMJ DP structure often exhibited one or more branch points from which usually three short branches extended into the x and y plane in a rather symmetric fashion (Fig. 2 A). Between these branches, baylike slots (here termed bays) were formed in which SVs were frequently found close to or in direct contact with the presynaptic plasma membrane (Fig. 2 A). However, images from this viewpoint were challenging to obtain.

Because EM reconstructions by tomography allowed rotation in any direction, we obtained tomograms of NMJ DPs from thick cross sections (250 nm). From the reconstructed volumes, we generated projections of DPs parallel to the AZ membrane (Fig. 2 B). This analysis confirmed the branched morphology of NMJ DPs as well as a previously reported network of tethers between the DP and SVs as well as between the SVs themselves (Fig. 1 E; Stigloher et al., 2011). DPs in cholinergic and GABAergic synapses shared similar structural features and size (Fig. 2, C and D). For all DP structures, we observed SVs proximal to the plasma membrane, which localized within the bays formed at DP branch points. We therefore propose these bays as putative release sites within the AZ.

Extended multimers of DPs in interneuron synapses

The activity of motoneurons is regulated by a network of command interneurons (de Bono and Maricq, 2005; Goodman, 2006). We collected longitudinal thin sections as well as tomographic reconstructions of DPs in such neuron–neuron synapses and found examples that were longer than NMJ DPs (Fig. 3 and Fig. S1). These larger DPs exhibited a similar organization of branch points and adjacent bays identical to the NMJ DPs. However, at the tip of one branch, a new branch point formed from which again three branches extended into the x and y plane, thus forming an
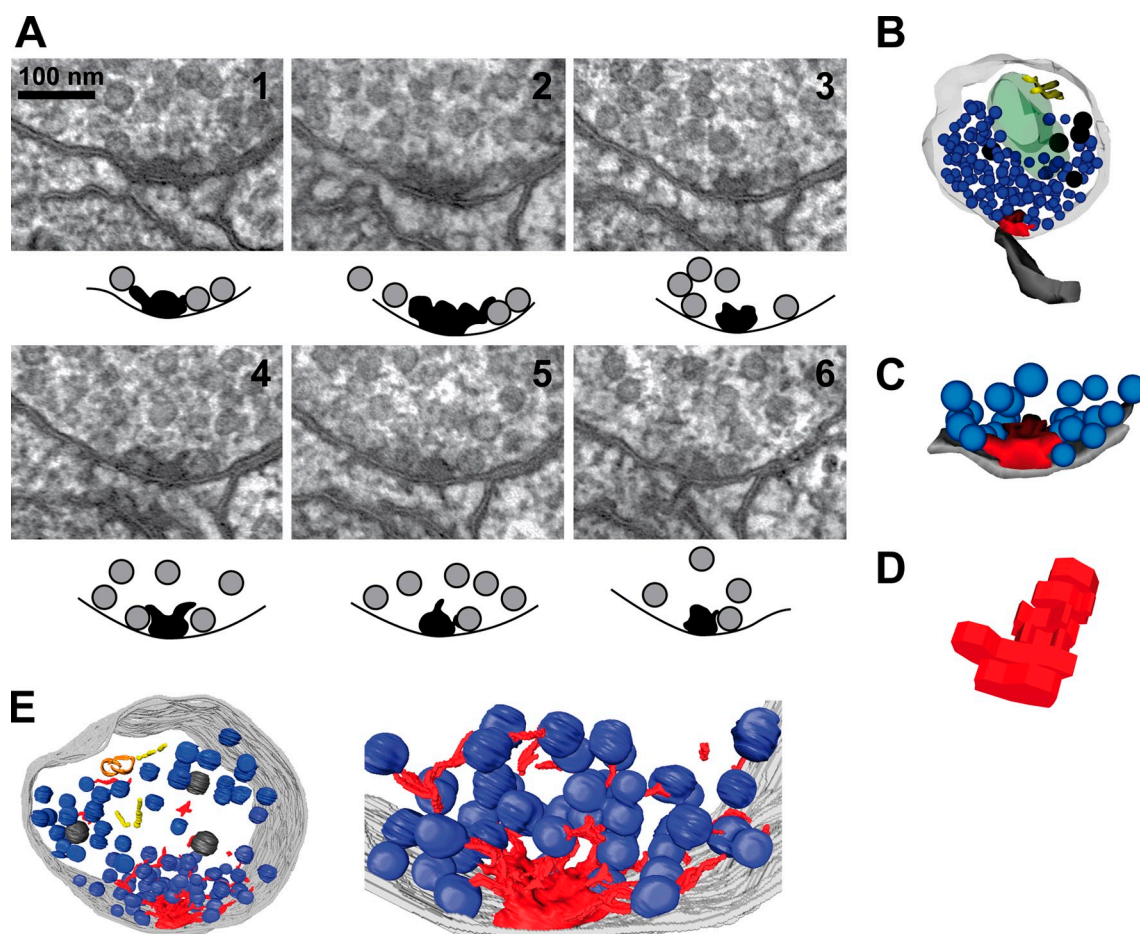
Figure 1. **3D structure of NMJ synapses by serial reconstruction of 40-nm-thin HPF EM sections and EM tomography.** (A) Six consecutive 40-nm sections (1–6) of a presynaptic cholinergic AZ with a schematic drawing of the DP and surrounding SVs below each section highlighting the tethers projecting from the DP to contact docked SVs. (B) 3D reconstruction from serial sections of a wild-type cholinergic NMJ synapse. The contacting postsynaptic muscle arm is shown in gray. (C) 3D model of the AZ reconstructed from serial sections 1–6. (D) 3D model of the DP only displayed as trace slabs to highlight the branch point. (E) Volume segmentation of a tomogram from a 250-nm-thick HPF/freeze substitution plastic section showing a cholinergic NMJ. Higher magnifications of the DP and close surrounding structures are shown on the right. Color codes are axon membrane (gray), the DP with emanating tethers (red), SVs (blue), DCVs (black), ER (orange), microtubules (yellow), and mitochondria (green).

elongated polymer of the NMJ DP structure following a common building principle. As seen at the NMJ, SVs were found within the bays close to the plasma membrane (Fig. 3 B and Fig. S1 A). This suggests that AZ DP components may polymerize to form an elongated ribbonlike DP with an increased number of release sites (bays). With its stereotyped branching pattern, the elongated DPs found at neuron–neuron synapses still resembled the ultrastructure of the basic DP prevalent at NMJs. This further suggests that elongated DPs might be generated by a multimerization or polymerization mechanism from the basic DP unit.

The AZ protein SYD-2 regulates the size of DPs

To understand the mechanism controlling AZ DP morphology, we analyzed proteins that have been implicated in synapse development. The multidomain protein SYD-2/Liprin-α has been shown to be involved in synaptogenesis by the recruitment of proteins that are components of the cytomatrix of the presynaptic AZ and SV docking machinery (Zhen and Jin, 1999; Dai et al., 2006; Patel et al., 2006). To investigate precisely how SYD-2 influences the architecture of NMJ DPs, we examined two *syd-2*

lof alleles, *ju37*, an early stop mutation, and *ok217*, a 2-kb deletion in the N terminus resulting in a stop codon after a frame shift (Fig. S2, A and C; Zhen and Jin, 1999; Wagner et al., 2009). Although the width of the DP in cross sections was not significantly different in either *syd-2* lof mutant (not depicted), the length of the DPs along the axons calculated from serial 50-nm sections was significantly shorter (Fig. 4). Specifically, a scatter plot of DP length revealed a significant shift toward shorter DPs ranging from 50 to 300 nm in *syd-2* lof mutants (mean of 123.8 ± 8.7 for *ju37* and 133.7 ± 8.1 for *ok217*), whereas wild-type DPs ranged between 100 and 350 nm (mean: 187.5 ± 8.5). These observations differ from the previous findings showing longer DPs in the *syd-2(ju37)* lof allele by Zhen and Jin (1999). However, their samples were prepared using glutaraldehyde chemical fixation, and the serial sections were 60–70 nm thick. It is possible that chemical fixation introduced artifacts to the DP morphology. Indeed, the earlier study reported that DPs in *syd-2(ju37)* were less electron-dense, suggesting diffuse DP materials possibly caused by slow fixation. Thus, the continuity of the DPs could not easily be resolved, and DP size may have been overestimated. Here, by rapid cryoimmobilization via HPF, freeze substitution,
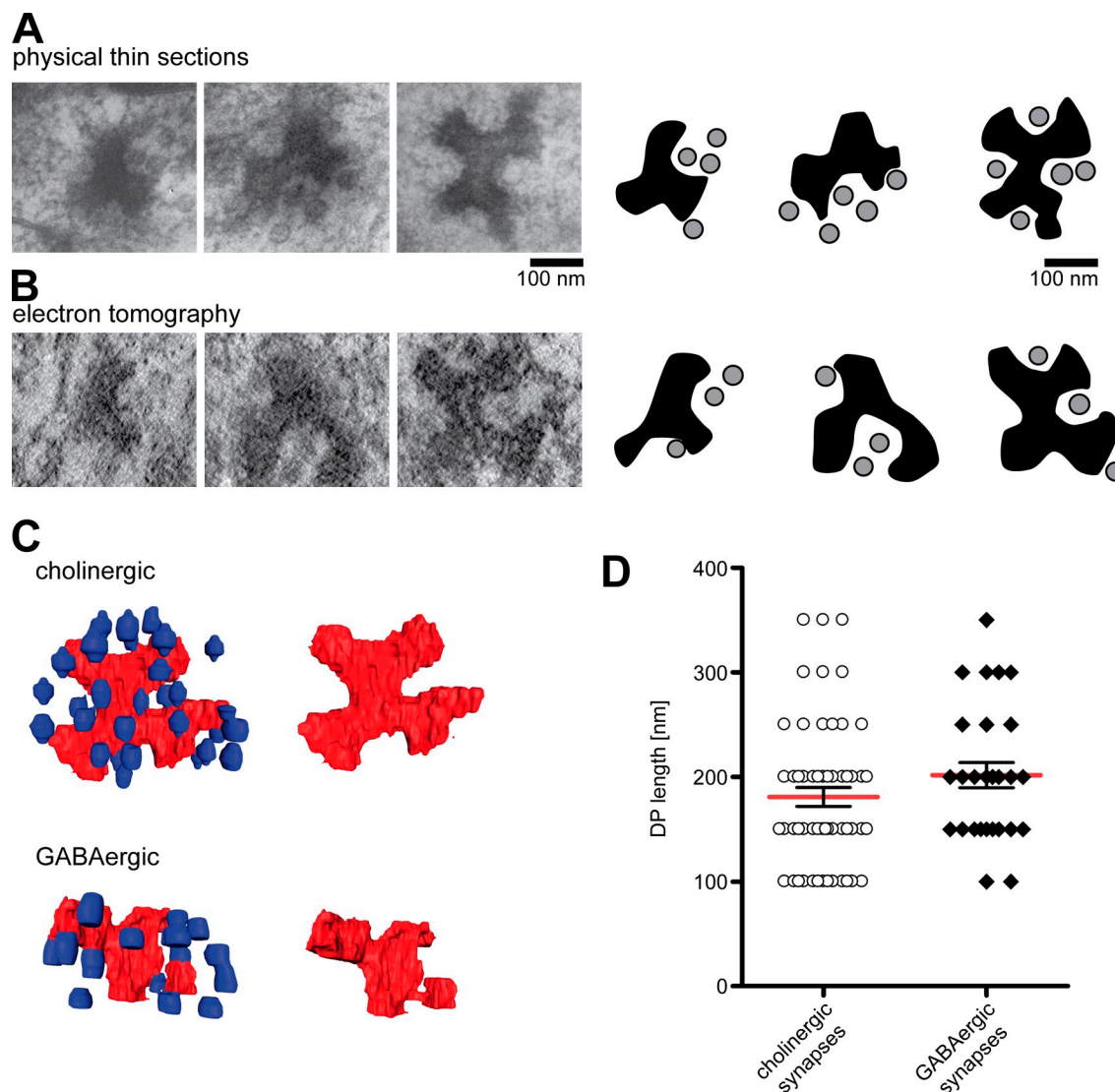
Figure 2. **The architecture of DPs at *C. elegans* NMJs.** (A) The branched structure of DP units was revealed by 50-nm ultrathin sections parallel to the AZ membrane. Bays formed at branch points often contained SVs in close contact with the presynaptic membrane. Schematic representations of the DP and SV within the bays are shown on the right. (B) Similar NMJ DP structures were observed in projections of HPF EM tomographic reconstructions. Schematic representations of the DPs and SVs within the bays are shown on the right. (C) Tomographic 3D reconstruction of NMJ DPs (red) with and without nearby SVs (blue) from cholinergic (top) and GABAergic (bottom) AZs. (D) The length of DPs was calculated from consecutive 50-nm-thin sections. Red lines indicate the means. Error bars represent the SEMs of DPs in wild-type cholinergic synapses (mean: 181.0 ± 9.0; $n = 58$) and GABAergic synapses (mean: 201.7 ± 12.0; $n = 29$). Statistics: Mann–Whitney test.

and thinner sectioning, we were able to minimize these artifacts and generate more reliable values for DP size. The reduction of DP size in *syd-2* lof mutants indicates that SYD-2 is required for normal DP morphology, possibly through its role in recruiting presynaptic cytomatrix proteins (Zhen and Jin, 1999; Patel et al., 2006). A *syd-2(ju487)* gof allele contains a point mutation that leads to a substitution of Arg184 to Cys within the highly conserved LH1 (Liprin homology 1) domain (Fig. S2 A; Dai et al., 2006). This mutated SYD-2 R184C protein bypasses the requirement of the upstream regulator SYD-1 during synapse assembly. We predicted that this *syd-2* gof allele would produce the opposite effect to the lof mutants. Consistent with this hypothesis, we found that *syd-2(ju487)* gof mutants exhibited significantly elongated DPs ranging between 50 and 650 nm (mean: 245.8 ± 15.7; Fig. 4).

To analyze how alteration in DP length affected the ultrastructure of NMJ DPs, we generated tomographic reconstructions of all *syd-2* mutants ($n = 3$). The complexity of DP morphology was reduced in *syd-2(ju37)* lof mutants because of the reduced size. Clear branch points were lost or hard to identify, but the formation of a bay structure was preserved (Fig. 5). Serial section reconstructions of synaptic terminals in the *syd-2* lof mutants showed the reduced size of DPs (see also Fig. 4) and reduced number of SVs surrounding the DP (Fig. 5). Tomographic reconstructions showed that the general DP morphology in *syd-2* gof mutants was similar to wild type. The typical branch points and bays were clearly visible. As quantified from serial sections, DPs in *syd-2* gof were significantly longer than wild-type DPs. 3D reconstruction of a synaptic terminal revealed that complexity of the DP was increased (Fig. 5), resembling elongated DPs in interneuron

A

B
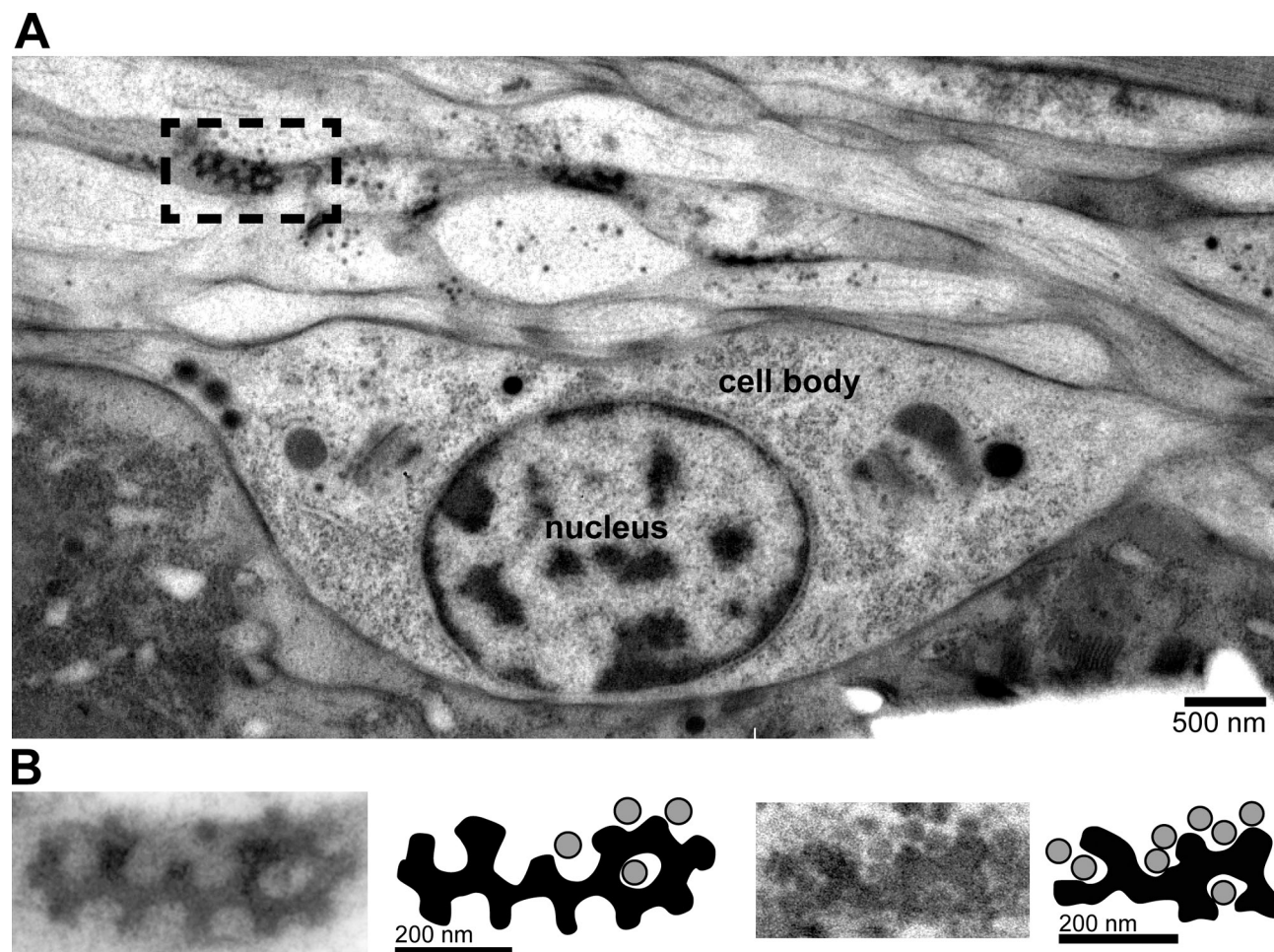
Figure 3. **DPs of neuron–neuron synapses resemble polymers of the NMJ DP unit.** (A) 50-nm HPF EM longitudinal section of the ventral nerve cord with an elongated DP of a neuron–neuron synapse (boxed area). (B) Neuron–neuron synapse DPs are larger and more complex but display a similarly branched morphology as NMJ DPs. Schematic representations of the same DPs and SVs within the DP bays are shown on the right.

synapses (Fig. 3). Similarly, these elongated DPs in *syd-2* gof exhibited regularly spaced branch points and bays (Fig. 5).

To get a larger overview of the morphology of motoneuron axons, we performed 10-µm reconstructions from serial 50-nm-thin sections of cholinergic and GABAergic neurons in the ventral nerve cord (Fig. 6). The number of SVs and DCVs at synaptic terminals was reduced in both *syd-2* lof alleles (DCV mean: 3.0 ± 0.9 and 3.1 ± 0.7; Fig. 7 C, SVs quantified) compared with wild type (DCV mean: 14.6 ± 2.7; Fig. 7 C, SVs). Within these reconstructions, we could also observe a lower frequency of DPs compared with wild type (Fig. 6), and DPs were smaller (quantified in Fig. 4). In contrast, *syd-2* gof mutants showed prominent DPs and normal vesicle clusters at presynaptic terminals (DCV mean: 9.4 ± 2.1; Fig. 6 and Fig. 7 C, SVs).

We could confirm these ultrastructural observations by the expression of the tagged SV-marker protein SNB-1 (synaptobrevin-1). SNB-1::GFP was expressed under a promoter specific for dorsal cholinergic (DA and DB) and GABAergic (DD) motoneurons, respectively (refer to methods for strains). SV clusters at axonal presynaptic AZs were easily visible as distinct puncta. The overall fluorescence and number of SNB-1::GFP puncta were reduced in *syd-2* lof alleles *ju37* and *ok217* (Fig. S3),

whereas *syd-2* gof mutants showed no or moderate effects. These results support the hypothesis that SYD-2 plays a role in DP higher-order assembly and/or stabilization.

syd-2 mutant animals show altered synaptic function

In line with the observed changes in DP morphology, *syd-2* mutants showed corresponding changes in sensitivity to the acetylcholinesterase inhibitor aldicarb. Specifically, *syd-2* lof animals exhibited mild resistance to aldicarb, consistent with reduced acetylcholine release. Further supporting this, *syd-2* mutants display a wild type–like sensitivity to levamisole, an agonist of postsynaptic nicotinic acetylcholine receptors (Fig. S4, A and B). In contrast, *syd-2(ju487)* gof animals were hypersensitive to aldicarb, consistent with enhanced release (Fig. S4 A). These data suggest that the alterations in synapse morphology have important functional consequences.

Based on previous studies of reduced SV clustering in *syd-2* lof mutants by in vivo imaging (Dai et al., 2006; Patel et al., 2006) and reduced SV tethering at NMJs shown by EM (Stigloher et al., 2011), we predicted that both lof and gof *syd-2* mutants would exhibit changes in vesicle localization within the AZ. Docked

Figure 4. **DP size depends on SYD-2 and its interaction with ELKS-1.** The length of DPs was calculated from consecutive 50-nm-thin axon cross sections as displayed in the schematic drawing. Red lines indicate the means. Error bars represent SEMs. *syd-2* loss-of-function (lof) mutant strains (*ju37* and *ok217*) have shorter DPs. The DP size of *elks-1(ok2762)* lof mutants is similar to wild type. Loss of both proteins (*syd-2(ju37)*; *elks-1(ok2762)*) results in a similar phenotype as in *syd-2* lof single mutants. In contrast, *syd-2(ju487)* gain-of-function (gof) mutant animals show elongated DPs. This DP elongation is dependent on ELKS-1. As in *syd-2(ju487)*; *elks-1(js816)* double mutants, longer DPs that are observed in *syd-2* gof single mutants are now reduced to the size of wild-type DPs. Number of synapses analyzed is indicated below each column. Statistics: Kruskal–Wallis test and Dunn's multiple comparison post test (*, $P \le 0.05$; **, $P \le 0.01$; ***, $P \le 0.001$). Columns without asterisks fail to reach significance.
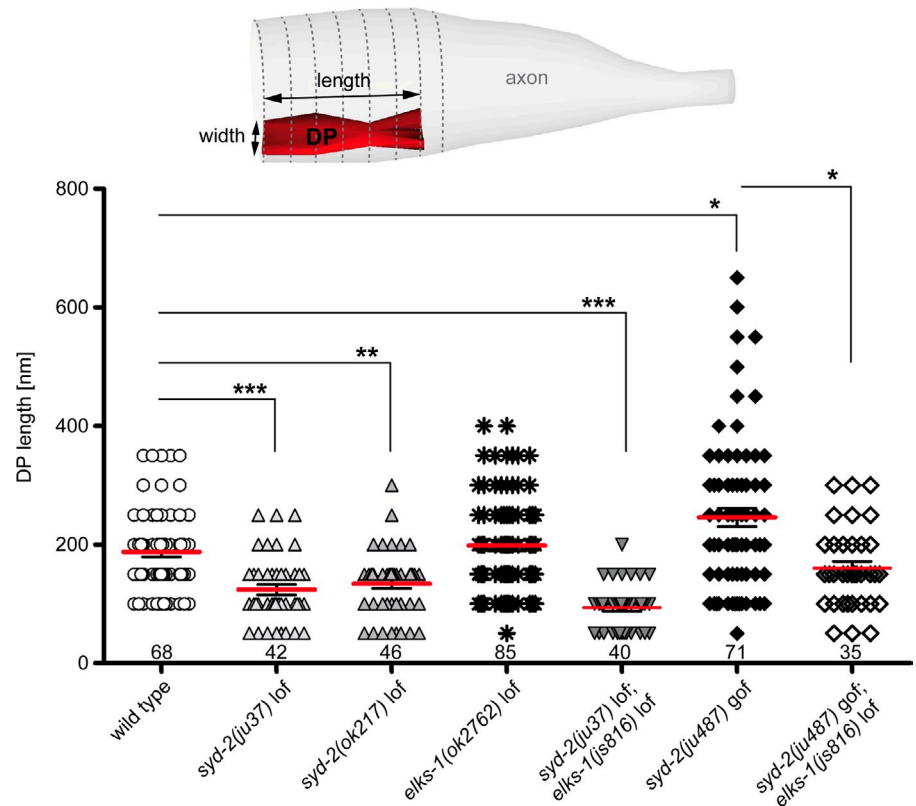
SVs within 120 nm of the DP were considered to represent the AZ, based on previous observations that immunogold staining for SYD-2, UNC-13, and Rab3-interacting molecule (RIM)/UNC-10 is restricted to this region and that the majority of docked SVs localize within this AZ region (Weimer et al., 2006; Stigloher et al., 2011). Fig. 7 A shows the distribution of docked SVs in the *syd-2* mutants relative to the DP. The number of docked vesicles within the AZ was significantly reduced in both *syd-2* lof mutant alleles (Fig. 7 B). This docking defect was consistent with previous tomographic analysis of *syd-2(ju37)* lof mutants (Stigloher et al., 2011), although direct comparison of docking distances to the DP cannot be made between these two studies, as docked vesicles were measured relative to the nearest DP protrusion in Stigloher et al. (2011), which cannot be detected in ultrathin sections. Therefore, by established convention, in the present analysis, docked vesicles were measured relative to the edge of the core DP (Weimer et al., 2006).

In contrast to the lof mutants, *syd-2* gof mutants did not reveal a significant alteration in the number of docked SVs within the AZ per thin section. However, because of the elongation of DPs in these mutants, the total number of docked vesicles per synapse was significantly increased (*syd-2(ju487)* gof 11.3 ± 1.6, $n = 30$ docked SVs/synapse) relative to the wild type (7.1 ± 0.6, $n = 33$; $P = 0.01$).

To determine how these morphological changes impacted synaptic function, we recorded basal electrically evoked responses and endogenous release from the NMJs of wild-type and *syd-2* mutants. The evoked response amplitudes of *syd-2(ok217)* lof mutants was significantly reduced (Fig. 8, A and C), as was the frequency of endogenous miniature events (Fig. 8, B and E).

Consistent with the normal levamisole sensitivity of these mutants, miniature event amplitudes were unaffected (Fig. 8 D), indicating that the reduced synaptic response of *syd-2* lof mutants reflects a presynaptic defect. Despite elongated AZ DPs and enhanced numbers of docked SVs, *syd-2(ju487)* gof mutants did not reveal a significant alteration in either basal evoked or endogenous synaptic transmission (Fig. 8, A–E).

To address the potential impact of the *syd-2* mutations on sustained release, we generated lines expressing channelrhodopsin in the cholinergic motoneurons, allowing the delivery of stimulation trains without incurring neuronal damage associated with repeat electrical stimulation (Liu et al., 2009). We first verified that blue light–activated channelrhodopsin could replicate the electrically evoked release phenotypes of the *syd-2* mutants (Fig. 8, F and H). We then analyzed synaptic release with a train of five stimuli delivered at 1 Hz. At this frequency, the NMJ response of wild-type worms underwent synaptic depression (Fig. 8, G and I–K). By comparison, the depression of *syd-2(ok217)* lof mutants was significantly exacerbated, whereas that of *syd-2(ju487)* gof mutants was significantly ameliorated. These data paralleled the opposing effects of the *syd-2* lof and gof mutants in aldicarb assays and mirrored changes in the number of DP-proximal docked SVs. Analysis of recovery times between successive channelrhodopsin evoked responses exhibited a similar trend: the *syd-2(ok217)* lof mutants recovering significantly slower than wild type, whereas the *syd-2(ju487)* gof mutants showing significantly faster recovery rates (Fig. 8 K). Together these data suggest that the respective changes in SV docking in *syd-2* lof and gof mutants impact the availability and replenishment of the readily releasable pool.

serial section reconstruction   **tomography**
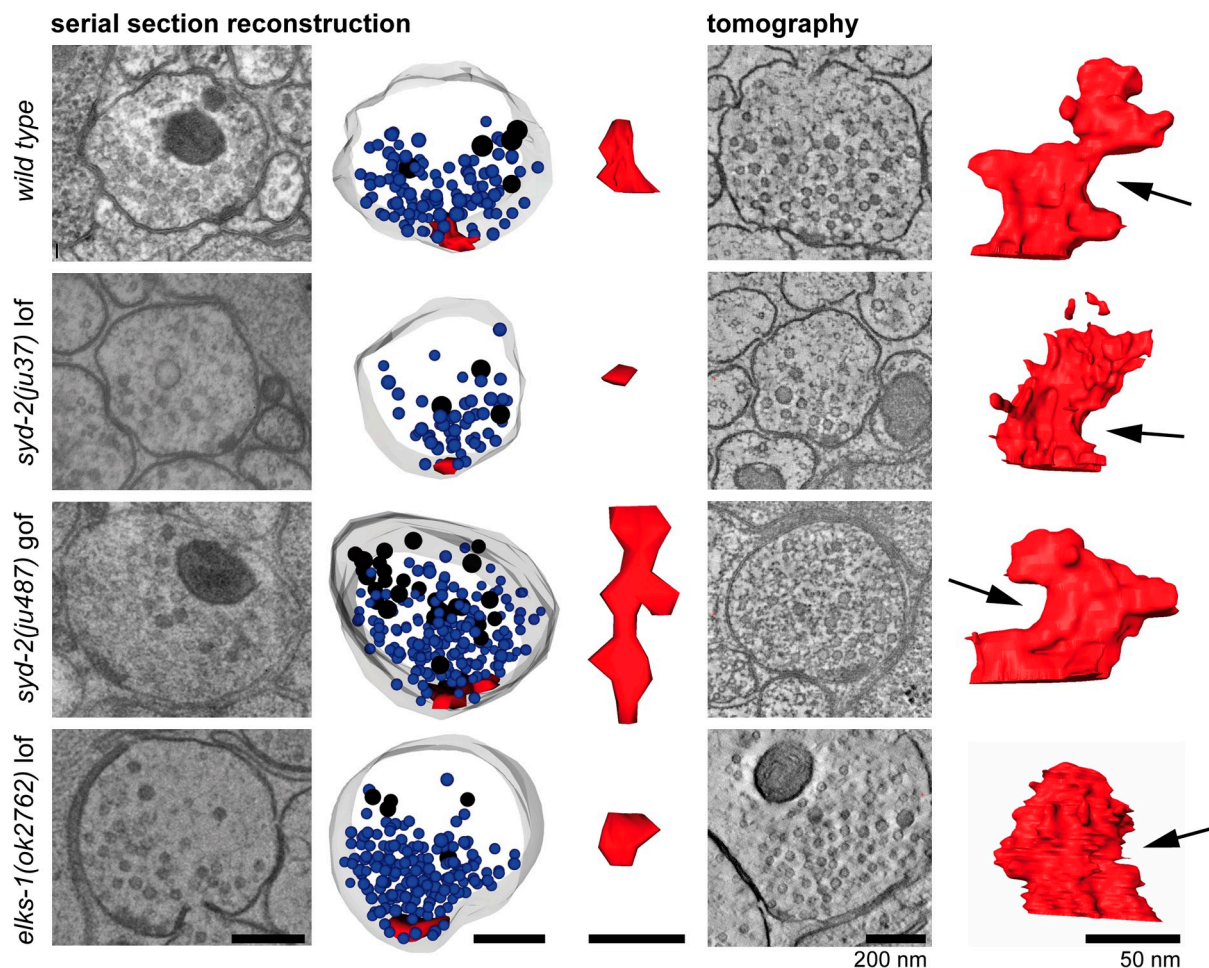
Figure 5. **3D morphology of NMJ DPs in wild-type and *syd-2* mutants.** 3D reconstructions illustrate the size of NMJ DPs and the clustering of SVs and DCVs around the DP. A representative 50-nm-thin section and the corresponding reconstruction from serial thin sections (50 nm) of a synaptic terminal and a top view of the DP alone are shown for wild-type, *syd-2*(*ju37*) lof, and *syd-2*(*ju487*) gof mutants. Axon membranes (gray), DPs (red), SVs (blue), and DCVs (black) were reconstructed. Bars, 200 nm. The number of SVs clustered around the DP is smaller in *syd-2* lof mutants, and the DP is typically smaller compared with wild type. DP size and vesicle clustering per cross section in *syd-2* gof and *elks-1* lof mutants is similar to wild type. Tomographic reconstructions from a 250-nm-thick section reveal the precise 3D ultrastructure of NMJ DPs (red). The branched structure is largely maintained in *syd-2* mutants, although lof mutants show decreased complexity caused by the reduced size of the DPs. Branch points and bays are clearly visible in wild-type and *syd-2* gof mutant DPs. Arrows highlight typical bay structures within DPs.

## The function of *syd-2* depends on the presence of ELKS-1

At HSN synapses, the SYD-2 gof mutation is able to bypass the requirement for SYD-1 in the presence of ELKS-1 (Dai et al., 2006). Therefore, we analyzed whether the increased NMJ DP size in *syd-2* gof mutants is also dependent on ELKS-1. First, we examined the AZ ultrastructure of two *elks-1*–null mutants (*ok2762* and *js816*; Fig. S2 B). DP ultrastructure in *elks-1* mutants was similar to wild type as was the DP length, typically ranging from 100 to 350 nm (mean: 198.2 ± 8.9; Fig. 4). Tomographic and serial section reconstructions of *elks-1* synapses demonstrated that SVs were also properly located within presynaptic terminals (Fig. 5) as *elks-1* mutants showed wild type–like SV docking and synaptic transmission (Fig. 8, A–E; Deken et al., 2005).

Coimmunoprecipitation assays have previously shown that ELKS-1 interacts more strongly with SYD-2 R184C gof protein than with wild-type SYD-2 (Dai et al., 2006). To investigate more precisely which region of SYD-2 specifically facilitates the binding to ELKS-1, we performed in vitro pull-down assays

and yeast two-hybrid experiments. The R184C gof mutation of SYD-2 is located within the highly conserved LH1 domain in the N-terminal coiled-coil domains (Fig. S2 A; Dai et al., 2006; Taru and Jin, 2011). Therefore, we expressed the N terminus (SYD-2 N, aa 1–517 or 515) including the LH1 domain of wild-type SYD-2 or SYD-2 R184C as well as full-length ELKS-1 tagged to either His6 or GST to perform in vitro pull-down assays. Western blot analysis of the eluted protein complexes clearly showed a stronger recruitment of ELKS-1 by SYD-2 N R184C than by wild-type SYD-2 N (Fig. 9, A and B).

The interaction between SYD-2 LH1 domain and ELKS-1 was further confirmed by yeast two-hybrid analysis. By using a minimal SYD-2 fragment (aa 91–207) comprising only the LH1 domain, we were able to narrow down the ELKS-1 binding site of SYD-2. Interestingly, we were only able to detect the SYD-2 LH1 R184C interaction with ELKS-1, whereas interaction with wild-type SYD-2 LH1 was too weak to be detected (Fig. 9 C). Thus, the enhanced recruitment of ELKS-1 by SYD-2 R184C gof seems to be mediated specifically by the LH1 domain.
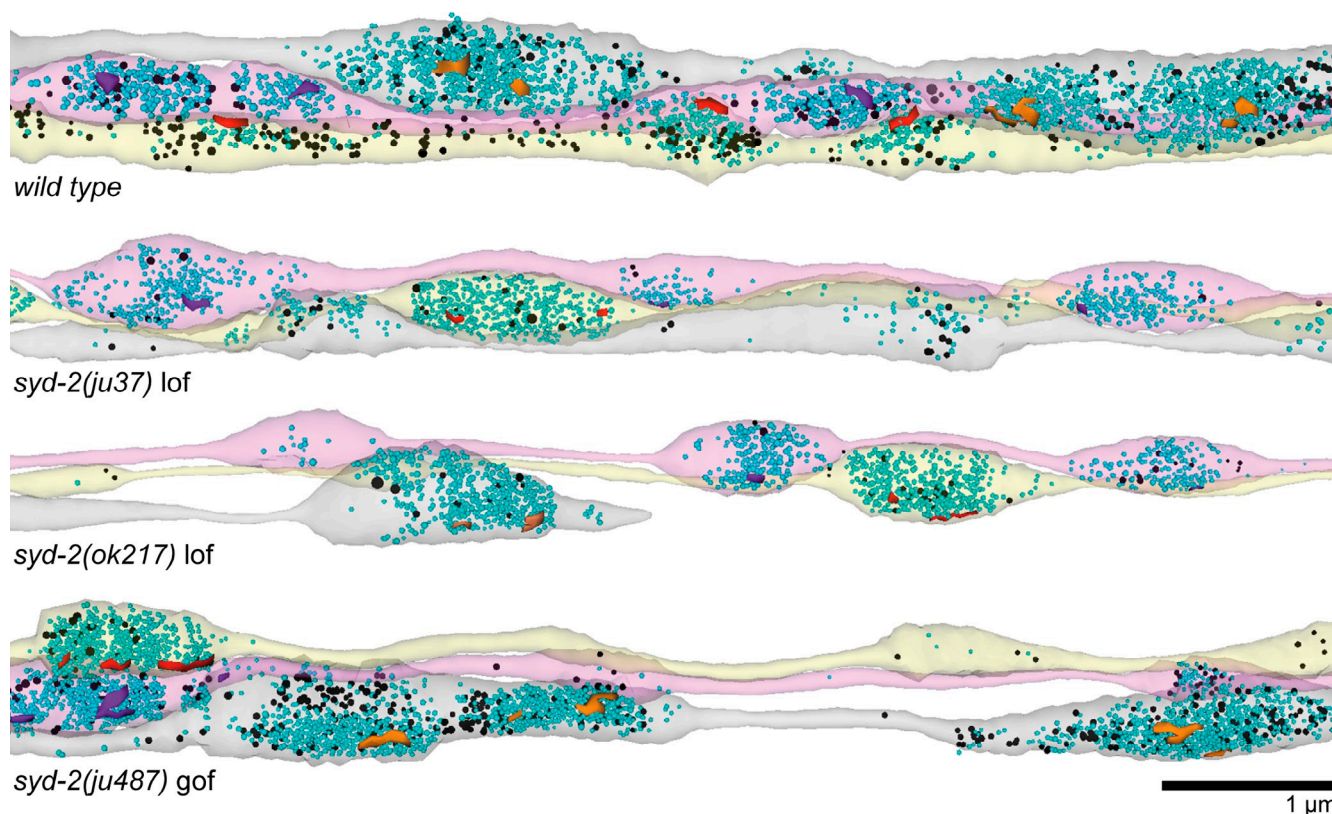
Figure 6.   **3D reconstructions of GABAergic and cholinergic motoneurons reveal altered vesicle clustering and reduced DP formation in *syd-2* lof mutants.**
The two cholinergic and one GABAergic axon within the ~10-μm ventral nerve cord were reconstructed from 50-nm serial sections (7.5 μm shown) for wild-type, *syd-2(ju37)* lof, *syd-2(ok217)* lof, and *syd-2(ju487)* gof animals. Cholinergic axons are colored yellow and magenta with the respective DPs in red and purple. GABAergic axons are colored gray with the respective DPs in orange. SVs are shown in blue, and DCVs are shown in black. In these reconstructions, the frequency of DPs is lower in the *syd-2* lof mutants (5 and 6 DPs/7.5 μm) compared with wild type and *syd-2(ju487)* gof (10 and 11 DPs/7.5 μm). In addition, DP size is reduced (refer also to Fig. 4), and less SVs cluster around the DPs (refer also to Fig. 7). Vesicle clustering in *syd-2* gof mutants is comparable to wild type.

To test in vivo whether the elongation of DPs at NMJs by SYD-2 gof was dependent on ELKS-1, we analyzed *syd-2; elks-1* double mutants by EM (Fig. 4). Double lof mutants *syd-2(ju37); elks-1(js816)* exhibited the same DP length and ultrastructure as *syd-2(ju37)* single mutants, suggesting that both proteins function in the same pathway (Fig. 4), whereas loss of ELKS-1 function in the *syd-2* gof background prevented the formation of elongated DPs observed in the *syd-2* gof single mutant (Fig. 4). This demonstrates that the ability of SYD-2 gof to polymerize larger DPs is strictly dependent on ELKS-1 and that the elongation of DPs is mediated by enhanced recruitment of ELKS-1.

A recent study has assigned the ability of homomeric dimer formation of SYD-2 to its LH1 domain using gel filtration and multiangle light scattering (MALS) experiments (Taru and Jin, 2011). We conducted similar experiments in this study with the mutant SYD-2 R184C LH1 domain (aa 91–207) at lower protein concentration. Dimers and even oligomers of SYD-2 R184C LH1 could be detected (Fig. 9 D, blue traces), whereas wild-type SYD-2 LH1 predominantly existed as monomer under the same conditions (Fig. 9 D, red traces). This suggests that the SYD-2 gof mutation can promote dimer formation and that these dimers or multimers have an increased affinity for ELKS-1. Therefore, SYD-2 most likely controls AZ DP size by modulating the affinity for ELKS-1 and thus the amount of ELKS-1 recruited to the AZ.

Discussion

The highly complex regulatory network at the presynaptic AZ orchestrates the finely tuned process of SV fusion. Upon stimulation, SVs are released within milliseconds, and the release machinery has to rapidly recruit new SVs to release sites at the AZ membrane. Additionally, the synaptic release machinery is also a highly dynamic system, which has to adjust to variations of stimuli strength and duration. The presynaptic DP is part of the protein scaffold of the AZ and is thought to be essential for SV recruitment. Rapid immobilization of intact *C. elegans* animals via HPF and subsequent fixation at low temperatures preserved synapse morphology and SV distribution in an almost native state (Rostaing et al., 2004). Using this method, the fine structure of DPs has been solved, revealing the existence of filamentous tethers emanating from the DP toward surrounding SVs at *C. elegans* NMJs (Fig. 1; Stigloher et al., 2011), possibly guiding SVs to their release site. The formation of these filaments as well as the number of docked vesicles is reduced in *syd-2* lof mutants, leading to a decrease in release from cholinergic motoneuron AZs. This effect is more pronounced with decreasing calcium concentration, supporting the proposal that primed SVs are coupled with local calcium signaling via SYD-2– and RIM-dependent tethering to the DP (Stigloher et al., 2011).
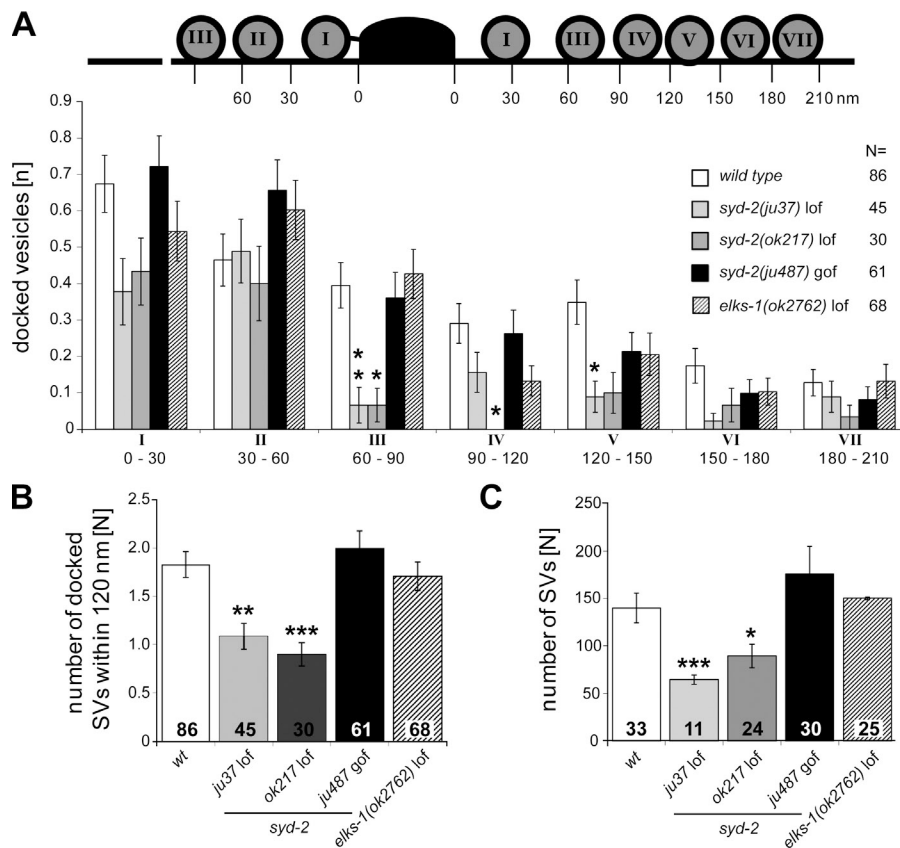
Figure 7. **SV docking at AZ membranes is reduced in *syd-2* lof mutants.** (A) The distribution of SVs docked to the plasma membrane in the AZ and peri-AZ around DPs was analyzed in the central 50-nm cross section profile for each DP (N, number of central cross sections analyzed). SVs were allocated to subsequent 30-nm bins along the membrane as indicated in the diagram. The mean number of SVs per bin is displayed on the bottom. (B) SV docking is reduced in close proximity to the DP. The number of SVs docked within 120 nm (bin I–IV) of the DP is significantly reduced in *syd-2* lof mutants. (C) The overall number of SVs present in all sections with a visible DP was analyzed. In *syd-2* lof mutants, the number of overall SVs per synapse is significantly reduced but not in *syd-2* gof and *elks-1* lof mutants. For each genotype, two or more independent animals were analyzed. The numbers in the bars represent the number (N) of synapse middle sections analyzed. Error bars represent SEMs. Statistics: Kruskal–Wallis test and Dunn's multiple comparison post test (*, $P \leq 0.05$; **, $P \leq 0.01$; ***, $P \leq 0.001$). Bars without asterisks fail to reach significance.

AZ DPs are organized as ultrastructural units that can be polymerized

However, the precise 3D ultrastructure of these DPs and their building principle remain to be determined. Here, we report that DPs in *C. elegans* cholinergic and GABAergic motoneurons follow a previously unknown building principle, with the smallest 3D ultrastructural unit resembling a three-pointed triadic structure. From a central branch point, three short branches extend planar along the presynaptic plasma membrane. Adjacent branches form baylike structures in which SVs are frequently found in contact with the subjacent plasma membrane (Fig. 2). We therefore propose that these bays define fusion sites where readily releasable SVs are located and released after presynaptic stimulation. Immunohistochemical studies in live animals and on EM sections have shown that AZ components, including the fusion machinery, are located within or close to the presynaptic DP (Wang et al., 1997; Tao-Cheng et al., 2000; Yeh et al., 2005; Weimer et al., 2006). Our proposed SV fusion sites would therefore be surrounded by a microenvironment in which the essential exocytic components including SNARE proteins and calcium channels are localized proximal to the SV. Interestingly, this bay-forming architecture has also been reported for the base of T-bar DPs in flesh fly *Sarcophaga bullata* NMJs (Feeney et al., 1998), suggesting that it may be an evolutionarily conserved architectural DP feature. Furthermore, we demonstrate the existence of longer DPs in ventral nerve cord and nerve ring neuron–neuron synapses (Fig. 3 and Fig. S1, A and B). However, these elongated DPs display the same 3D ultrastructural elements of spaced branch points and bays. This suggests that DPs in all presynaptic AZs in *C. elegans*

may follow a common building principle and that longer DPs may be multimers or polymers of the NMJ DP unit. Therefore, it is likely that mechanisms exist to control the extent of the polymerization or multimerization process at a given presynaptic AZ. In this respect, it is interesting to note that inactivation of the *Drosophila* neuronal SAD-1–related serine/threonine kinase (SRPK79D) leads to ectopic accumulations of the AZ protein BRP in elongated structures (Nieratschker et al., 2009), which resemble *C. elegans* long DPs in their 3D ultrastructure. These ectopic AZ-like aggregates may result from an aberrant polymerization of DP units in *Srpk79D* mutants, suggesting that such a polymerization process might be evolutionarily conserved. In agreement with this, EM tomography analysis of frog NMJs also shows a similar zipperlike elongated DP topology that might have resulted from a linear polymerization process of DP units (Harlow et al., 2001).

The AZ DP polymerization is controlled by the activity of SYD-2/Liprin-α

The polymerization process of AZ DPs must be tightly controlled by regulatory factors because NMJ DPs typically do not reach the complexity that can be observed at neuron–neuron synapses in *C. elegans*. Furthermore, ectopic aberrant DP polymerization has to be prevented. To understand how the DP polymerization process is regulated, we analyzed factors that are known to function in synapse formation. In addition to previous studies that have implicated *C. elegans* AZ protein SYD-2/Liprin-α in synaptogenesis (Zhen and Jin, 1999; Dai et al., 2006; Patel et al., 2006), we found that SYD-2 plays a central role in promoting
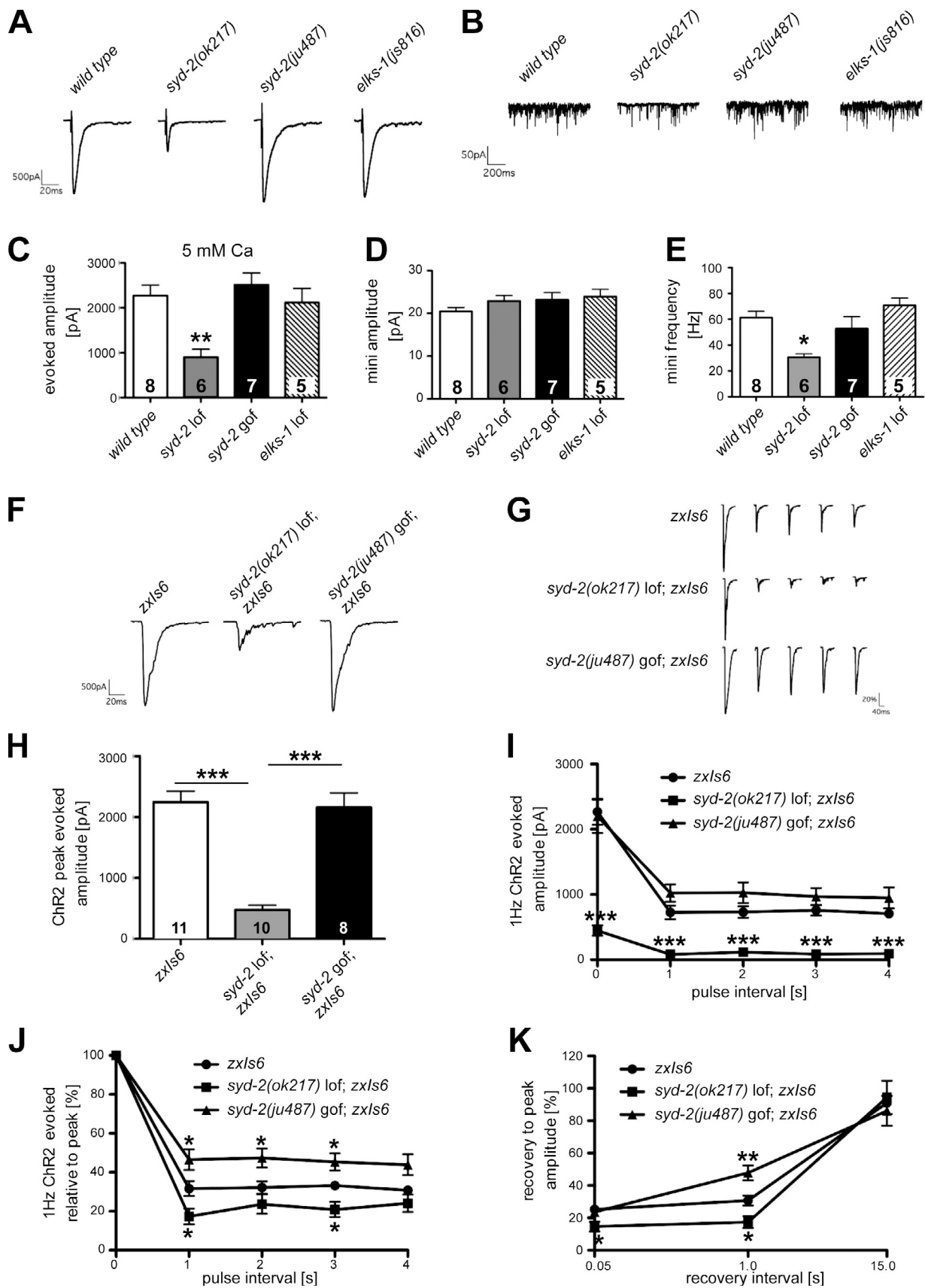
Figure 8. **syd-2 lof and gof mutants exhibit opposing functional changes.** (A and B) Representative electrically evoked (A) and mini (B) traces recorded from the NMJs of dissected animals are shown for wild-type, *syd-2(ok217)* lof, *syd-2(ju487)* gof, and *elks-1(js816)* lof mutants (similar recordings were obtained from a total of 8, 6, 7, and 5 worms from each respective strain as plotted in C). (C) The mean electrically evoked current amplitude is reduced in the
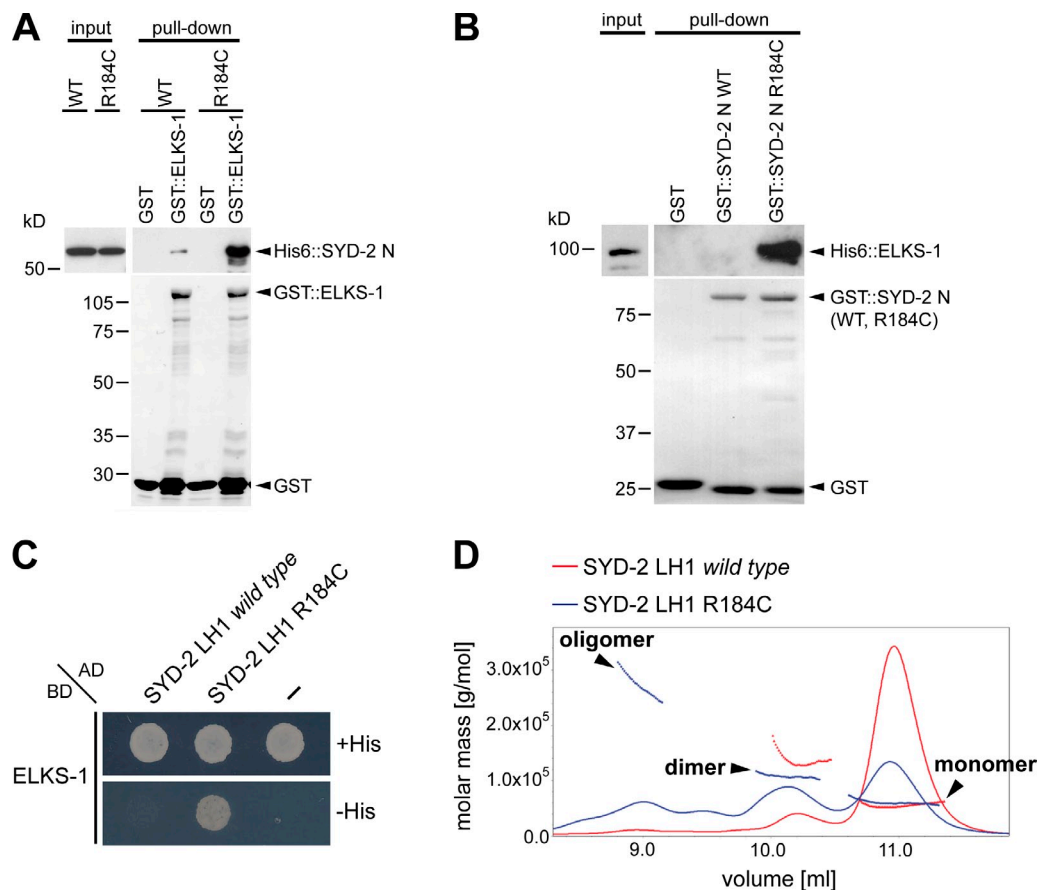
Figure 9. **The SYD-2 gof protein R184C substitution enhances oligomerization and ELKS-1 recruitment in vitro.** (A and B) Interaction between His6::SYD-2 N (aa 1–517) and GST::ELKS-1 (A) or between His6::ELKS-1 and GST::SYD-2 N (aa 1–515; B) was examined by in vitro pull-down assay. Interaction of the SYD-2 N-terminal region and ELKS-1 was enhanced by the SYD-2 R184C substitution. Proteins were analyzed by Western blotting with anti-His6 antibody (top) and by Ponceau S stain (bottom). (C) Yeast two-hybrid assay with ELKS-1 protein fused to the yeast Gal4p DNA binding domain (BD) and SYD-2 LH1 (aa 91–207) fused to the Gal4p activation domain (AD). Interactions between ELKS-1 and SYD-2 LH1 R184C are stronger compared with wild-type SYD-2 LH1 (below detection level). (D) The oligomerization of SYD-2 LH1 (aa 91–207) fused to MBP was analyzed by gel filtration with size exclusion column and MALS. SYD-2 LH1 wild-type protein is mainly detected as monomer (red lines), whereas SYD-2 LH1 R184C preferentially forms dimers or higher oligomers (blue lines). The chromatogram indicates the differential reflective index and molecular mass (grams/moles) for each peak calculated from light scattering data. WT, wild type.

DP polymerization. Lof in SYD-2, which can dimerize (Taru and Jin, 2011) and interact with multiple other AZ proteins, including ELKS-1/ELKS (Ko et al., 2003) and RIM1 (Schoch et al., 2002), resulted in a lower number and significantly shorter NMJ DPs (Fig. 4, Fig. 6, and Fig. S3). However, most NMJ DPs were still present, and their overall 3D ultrastructure with the formation of bays was preserved in at least one DP of each *syd-2* lof mutant (Fig. 5). In addition, we found that a gof mutation in SYD-2 promotes elongation of NMJ DPs, which now resemble the more elaborate DPs normally found at neuron–neuron synapses. Our analysis of *syd-2* gof DP length suggests that the elongation of the basic 100–150-nm DP unit (Fig. 2, A and B) does not happen by multimerization of discrete DP units but rather by incremental addition of DP material according to the specific architectural concept resembling the basic DP unit (Fig. 2 D). Therefore, we currently favor an underlying model of DP polymerization rather than a mechanism in which the multimerization of single DP units occurs. As formation of DPs

syd-2 lof mutant compared with wild-type animals, whereas *syd-2* gof mutant and *elks-1* lof mutant responses are similar to wild type. (D) Miniature evoked junctional current amplitudes are comparable. (E) Only the miniature frequency of *syd-2* lof mutants is reduced compared with wild type. To examine trains of stimuli, transgenic animals of the same wild-type and mutant strains were generated expressing channelrhodopsin2 (ChR2 H134R) in cholinergic motoneurons (*zxIs6*). (F and H) Blue light activation of worms grown on retinal produce similar peak evoked amplitudes compared with electrically evoked preparations as shown in the representative traces (recordings were obtained from a total of 11, 10, and 8 worms of the wild-type, *syd-2(ok217)*, and *syd-2(ju487)* strains, respectively) and quantified in H. (G and I–K) 1-Hz trains of five responses normalized to the first peak show more pronounced depression in *syd-2(ok217)* lof mutants (n = 9 independent repeat experiments) when compared with wild type (n = 10), whereas *syd-2(ju487)* gof exhibit less fatigue (n = 8), graphed as absolute ChR2-evoked amplitudes in I and normalized values in J. The rate of recovery between consecutive ChR2 responses of varying interval (50 ms, 1 s, and 15 s), plotted as a percentage of the initial evoked response amplitude in K, demonstrates a slower recovery in *syd-2 (ok217)* lof mutants (n = 10, 10, and 9 worms for 50-ms, 1-s, and 15-s recovery time points) and faster recovery in *syd-2(ju487)* gof mutants (n = 8, 8, and 9 worms for each recovery time point) relative to wild type (n = 10, 11, and 10 worms for each recovery time point). Error bars represent SEMs. Statistics: Mann–Whitney test (*, $P \leq 0.05$; **, $P \leq 0.01$; ***, $P \leq 0.001$). Columns without asterisks fail to reach significance. *n* are indicated in each bar.

at NMJs is not abolished in SYD-2 lof mutants, but DP size is reduced, we suggest that in addition to contributing to the formation of AZs, SYD-2 regulates DP size and formation of fine structures that are essential for the proper recruitment of SVs to the AZ membrane.

Is the regulation of DP size by SYD-2 a form of synaptic plasticity?

We show here that even DPs at NMJ AZs, which normally contain small DPs, can be elongated by increasing SYD-2 activity. This suggests that all AZs have the ability to form longer DPs dependent on SYD-2 activity. Furthermore, our aldicarb data and electrophysiological analyses of *syd-2* mutants suggest that SYD-2 plays an important functional role in determining synaptic strength. In the case of *syd-2* lof mutants, we observed fewer docked SVs associated with smaller DPs, which could account for the release defect. However, release may also be impacted by a reduction in synaptic number in these mutants, although this observation is based on quantification of fluorescently tagged SV clusters that may fall below detection levels as a result of reduced SV density. Consistent with the possibility that there is an SV detection limitation, the localization of another DP component UNC-10/RIM1 is not affected in *syd-2(ju37)* lof mutants (Deken et al., 2005). This supports the notion that synapses are still present but smaller in the absence of SYD-2. In the *syd-2* gof mutants, the enhanced release appears to be a consequence of larger DPs that support increased numbers of docked SVs because the overall number of synapses was not impacted (Fig. S3).

SYD-2–dependent changes in DP size and function may be a plasticity mechanism used to dynamically adjust synaptic transmission to stimulus intensity or to maintain network homeostasis by regulating the size of release sites (Fig. S5). The activity of SYD-2 could then be regulated in a neuron-specific manner by regulating expression levels or stability of SYD-2 or the activity of negative or positive regulators. In *Drosophila*, Liprin-α/SYD-2 levels were shown to be modulated by the anaphase-promoting complex/cyclosome (van Roessel et al., 2004), whereas in *C. elegans*, positive (SYD-1) as well as negative regulators (RSY-1) of SYD-2 have been identified (Hallam et al., 2002; Patel and Shen, 2009).

Does SYD-2 regulate AZ DP size by recruitment of ELKS-1?

The requirement of ELKS-1 for SYD-2 functionality was first indicated by an in vivo study in the *C. elegans* HSN synapses (Dai et al., 2006). Here, we provide additional evidence that ELKS-1 specifically interacts with the N-terminal LH1 domain of SYD-2 and thereby may enhance SYD-2 function (Fig. 9, A–C). This interaction is most likely of low affinity because it was hard to detect by in vitro protein binding and the yeast two-hybrid assays (Fig. 9, A–C). However, once SYD-2 was activated by the R184C gof mutation, leading to extensive dimer and multimer formation (Fig. 9 D), the affinity for ELKS-1 was highly increased (Fig. 9, A–C). This increased affinity may lead to a stronger recruitment of ELKS-1 to the AZ and subsequently increased polymerization of the DP. Accordingly, the increased elongation of DPs in *syd-2* gof mutants was lost in *syd-2(gof); elks-1* double mutants

as judged by serial EM reconstructions (Fig. 4). However, it should be noted that the genetic interaction between *elks-1* and *syd-2* was only apparent in the *syd-2* gof mutant background; no effect of *elks-1* alone on DP size was observed. Therefore, the formation of presynaptic DPs is not affected by ELKS-1, but polymerization into more complex structures is impaired without ELKS-1. We therefore propose that ELKS-1 functions in DP assembly through its recruitment by SYD-2, which is dependent on the SYD-2 dimerization state (Fig. S5). Thus, SYD-2 dimer formation most likely promotes an enhanced stability of AZ protein complexes that then leads to increased DP polymerization (Taru and Jin, 2011). Interestingly, in nonneuronal COS7 cells, Liprin-α1 has been reported to be required for lamellipodia formation by controlling the talin-mediated activation and polymerization of peripheral integrin β1 for cell spreading and motility (Asperti et al., 2009). Therefore, our study might be a first step toward unifying the molecular roles of SYD-2/Liprin-α as a scaffold required to assemble a molecular network controlling the productive polymerization of elongated structures in different systems and cell types. Liprin-α activity would thereby be required to shift a dynamic equilibrium to assemble and recruit scaffold components needed for polymerization. Thus, the activity status of SYD-2/Liprin-α might be used to transiently recruit scaffolds such that low affinity interactions are stabilized to be productive.

Materials and methods

Strains

If not otherwise stated, strains were grown at 20°C as previously described (Brenner, 1974). Strains used in this study were the wild-type Bristol N2, CZ900 *syd-2(ju37)* (Q397stop point mutation [Zhen and Jin, 1999]; primers 5′-CACAACGCACCGATCA/3′-CTTGCATTCGTTCTTTGA), ZM607 *syd-2(ok217)* (2-kb deletion leading to an early stop after aa 200 [Fig. S2]; primers 5′-TTGCATCTGCAAAAGAAACG/3′-GCTCCGAACGAAAGAA-GTTG), CZ4601 *syd-2(ju487)* (R184C point mutation; primers 5′-AGAT-GAAGAGATTGTCGAG/3′-GGTATGTGATGTATTCTCG), VC2392 *elks-1(ok2762)* (deletion mutation; primers 5′-CGAATGGAACTCCGAGA-ACG/3′-CTTGCACAAGATCCCGATTC), VC223 *tom-1(ok285)* (deletion mutation; hypomorphic allele) ordered from the Caenorhabditis Genetics Center (College of Biological Sciences, University of Minnesota), and CZ5971 *elks-1(js816);syd-2(ju487)*, CZ5821 *elks-1(js816);syd-2(ju37)*, CZ333 *juls1 [Punc-25::SNB-1-GFP] IV*, a marker for presynaptic SV clusters in GABAergic motoneurons (Hallam and Jin, 1998), CZ6234 *syd-2(ju37);juls1[Punc-25::SNB-1-GFP]*, CZ4231 *syd-2(ok217);juls1[Punc-25::SNB-1-GFP]*, CZ4576 *syd-2(ju487);juls1[Punc-25::SNB-1-GFP]*, and GQ707 *zxIs6 V [Punc-17::ChR2(H134R)::YFP;lin-15+]* expressing a *ChR2 (channelrhodopsin2)*-YFP fusion protein in cholinergic motoneurons (Liewald et al., 2008). NM2775 *elks-1(js816)* (a deletion that results in a premature stop at aa 292 [Fig. S2; Deken et al., 2005]; primers: 5′-CTCACCACAGCTTTAGAATCCG/3′-CTCA-CCGCTTCTTTGCTTGCAC) and NM1657 *unc-10(md1117)* X (8,601-bp deletion that removes the entire UNC-10 coding region; primers 5′-CGCCC-TCTTTCTCTTTCCTTAC/3′-AGCCTACTAACCCATTTCTCACTG) were provided by M. Nonet (Washington University School of Medicine, St. Louis, MO). J. Kaplan (Massachusetts General Hospital, Boston, MA) provided *nuls152 [Pttx-3::mRFP; Punc-129::GFP–SNB-1]II*, which marks presynaptic SV clusters in a subset of dorsally projecting DA and DB motoneurons (Sieburth et al., 2005). GQ751 *syd-2(ok217);zxIs6*, GQ752 *syd-2(ju487); zxIs6*, GQ171 *syd-2(ju37)X;nuls152 [Pttx-3::mRFP;Punc-129::GFP-SNB-1]II*, GQ172 *syd-2(ok217)X;nuls152 [Pttx-3::mRFP;Punc-129::GFP-SNB-1]II*, and GQ173 *syd-2(ju487)X;nuls152 [Pttx-3::mRFP;Punc-129::GFP-SNB-1]II* were generated in this study.

HPF/freeze substitution

A 100-μm-deep aluminum platelet (Microscopy Services) was filled with *Escherichia coli* OP50 suspension. About 20 young adult worms were transferred into the chamber and immediately frozen using a HPF machine (HPM 10; Bal-Tec). Freeze substitution was performed in an automatic free

substitution system (EM AFS; Leica) at −90°C for 100 h in 0.1% tannic acid and another 40 h in 2% OsO$_4$ (each weight/volume in dry acetone) slowly increasing temperature, according to Rostaing et al. (2004).

EM
40- or 50-nm sections were cut using an ultramicrotome (UC6; Leica). Ribbons of sections were transferred on Formvar-coated copper slot grids. The grids were placed for 30 min on drops of 4% (wt/vol) uranyl acetate in water and then washed in distilled water. After air drying, the grids were placed on drops of lead citrate (Reynolds, 1963) for 2 min in a CO$_2$-free chamber and rinsed in distilled water. Micrographs were taken with a 1,024 × 1,024–pixel charge-coupled device detector (Proscan CCD HSS 512/1024; Proscan Electronic Systems) in a microscope (EM 902A; Carl Zeiss) operated in the bright-field mode.

Serial section reconstruction
Consecutive images of serial sections were imported into reconstruct mode (Fiala, 2005) and aligned in the rigid mode using the alignment tool with traces in adjacent sections and manual fine alignment. Vesicles were traced with the circle tool in the section of their largest diameter and reconstructed as sphere. All other components (DP and membrane) were traced in all sections using the closed point-by-point drawing tool and reconstructed as Boissonnat surface with maximal facets. For the 10-μm reconstructions, z traces were generated through the center of the axons and smoothened with a moving mean filter length of 10.

Electron tomography
250- and 350-nm cross sections were poststained with uranyl acetate and lead citrate (see EM), respectively. Gold particles were applied as fiducial markers on both sides of the section. Carbon coating was applied on both sides. Two tilt series shifted 90° against each other were recorded on an electron microscope (EM 912; Carl Zeiss) at 120 kV and 20,000× or on a transmission electron microscope (4000EX; JEOL) with a 4K × 4K lens-coupled charge-coupled device camera at 400 KV and 25,000× each with 2° increment from −60 to 60°. Irradiation at all tilt angles was performed beforehand to limit specimen deformation during the image collection process. Rough alignment of the two tilt series was performed with IMOD software package (Kremer et al., 1996). Fine alignment and reconstruction was performed using the TxBR package (Lawrence et al., 2006). Volume segmentation was performed by manual tracing using Amira (FEI).

Fluorescence analysis
Localization of fluorescent puncta in dorsal cord axons was analyzed via confocal microscopy. Live animals were placed on 2% agarose pads and immobilized with 50 mM Na-azide in M9 buffer. All images were obtained on an inverted confocal microscope (SP2; Leica) using a 63×, NA 1.32 oil immersion objective at 20°C. Image stacks were captured, and maximum intensity projections were obtained using LCS software (Leica). The posterior part of the dorsal nerve cord was imaged in young adult animals when oriented toward the objective, using the same settings for all of the images obtained. Total fluorescence in maximum stack projections was analyzed using the polygon selection for ImageJ software (National Institutes of Health).

Western blotting
For SYD-2 protein quantification, mixed-stage worm extracts were prepared as reported previously (Eimer et al., 2007). In short, six large 9-cm plates containing worms of all stages from egg to young adult were rinsed off and washed two times with M9 buffer, pelleted by centrifugation, and resuspended in 400 μl homogenization buffer including protease inhibitor (cOmplete, EDTA-free Protease Inhibitor Cocktail Tablets; Roche). Samples were frozen at −80°C for 30 min and sonicated, and total protein content was measured. About 50 μg of total protein extracts per strain was loaded and separated on 7.5% SDS-PAGE gel, blotted onto nitrocellulose membrane, and probed against SYD-2 and actin. The polyclonal goat antibody against the N-terminal region of SYD-2 (Santa Cruz Biotechnology, Inc.) and the polyclonal rabbit antibody (Sigma-Aldrich) were used at 1:500 dilutions. Peroxidase-coupled secondary antibodies (donkey anti–goat [Santa Cruz Biotechnology, Inc.]; goat anti–rabbit [The Jackson Laboratory]) were used at 1:10,000 dilutions. The signal was revealed with a camera (LAS-3000; Fujifilm). These experiments were executed at least twice.

Aldicarb assay
3-cm agar plates were seeded with a drop of 50 μl OP50 in the center of the plate and incubated overnight at 37°C. Aldicarb (Sigma-Aldrich) was dissolved in 70% ethanol to 1.5 mM and spread over the seeded plates.

Ethanol evaporated for ∼30 min from open plates, which were then immediately used. 30 young adult worms were transferred onto the bacteria lawn, and paralyzed worms were scored every 30 min. Animals were considered completely immobilized when the nose and tail showed no movement after touching with a worm pick (n = 4 independent repeat experiments).

Levamisole assay
Levamisole was added to the liquid agar to give a final concentration of 0.2 mM before plates were poured and kept at 4°C. Before use, plates were seeded with a drop of 50 μl OP50 in the center of the plates and incubated at 37°C overnight to grow a thin bacteria lawn. 10 young adult animals were placed on the plates, and motility was checked every 10 min by tapping the plates and body touches with a worm pick. Animals were considered completely immobilized when no nose or tail movement was detectable (n = 3 independent repeat experiments).

Biochemistry
The following bacterial expression constructs for GST fusion and His6-tagged proteins were generated using Gateway cloning system (Invitrogen) as described in the manufacturer's protocols: ELKS-1/pGEX-6P (pCZGY688), ELKS-1/pRSET B (pCZGY659), SYD-2 N (1–517) wild type/pRSET (pCZGY682), and SYD-2 N (1–517) R184C/pRSET (pCZGY683). The SYD-2 fragment (aa 1–515) was cloned between BamHI and SalI sites of a modified pGEX-6P vector to generate SYD-2 N wild type/pGEX-6P (pCZ757) or SYD-2 N R184C/pGEX-6P (pCZ758). SYD-2 91–207 was cloned between EcoRI and BamHI sites of a pMAL-c2 vector to generate SYD-2 91–207/pMAL-c2 or SYD-2 91–207 R184C/pMAL-c2 (gifts from R. Jin, Sanford-Burnham Medical Research Institute, La Jolla, CA). Plasmids were confirmed by sequencing.

Recombinant GST, His6, and maltose binding protein (MBP) fusion proteins were produced in E. coli BL21(DE3) with pGEX-6P, pRSET, and pMAL-c2 plasmids incubating for 16 h at 22°C in the presence of 0.1, 0.5, and 0.3 mM IPTG, respectively. Proteins were extracted by sonication in PBS, pH 7.4, with 0.1% Triton X-100, 1 mM DTT, and protease inhibitors (Roche). For GST pull-down analysis, GST fusion proteins in supernatant were immobilized to glutathione-Sepharose (GE Healthcare), incubated with His6 proteins in supernatants for 3 h at 4°C, and washed four times. Protein complexes were eluted and analyzed by Ponceau S staining and Western blotting using a chemiluminescent substrate (SuperSignal West Femto; Thermo Fisher Scientific) and mouse monoclonal anti-His6 (EMD Millipore) antibody. For gel filtration analysis, MBP-LH1 and MBP-LH1 (R184C) were purified with Amylose resin (New England Biolabs, Inc.), and 40 μg proteins was applied to an HPLC (1100; Agilent Technologies) with PROTEIN KW-803 column (Shodex) equilibrated with 20 mM potassium phosphate, pH 6.8, and 50 mM sodium chloride at a 0.5-ml/min flow rate, detected by a MALS instrument (DAWN HELEOS 8+; Wyatt) and a refractive index detector (Optilab rEX; Wyatt). These experiments were executed twice.

Yeast two-hybrid assay
PCR amplification and PCR mutagenesis of the SYD-2 LH1 domain and ELKS-1 from a C. elegans cDNA library (ProQuest; Invitrogen) were performed using PfuUltra II Polymerase (Agilent Technologies). Wild-type LH1 was amplified with primer 5′-CCCCATATGGCACCGGTACAGGAACTTC-AAACAATGACG-3′ (oGQ 2183) introducing 5′ NdeI and AgeI restriction sites and 5′-CCCCTCGAGTCAGCGGCCGCCCGAATTCTCATCTCCTT-TTGT-3′ (oGQ 2237) primer introducing 3′ NotI, a STOP, and an XhoI restriction site. The fragment was cloned between AgeI–XhoI sites of pGADT7 and pGBKT7 vectors (Takara Bio Inc.) for yeast two-hybrid analysis. The SYD-2 R184C mutation corresponding to the syd-2(ju487) gof allele was introduced into the SYD-2 LH1 domain by PCR mutagenesis and also cloned into pGADT7 and pGBKT7 vectors between AgeI–XhoI sites. Plasmid constructions were confirmed by sequencing.

Amplification and cloning procedures were the same for the ELKS-1 construct. Amplification of elks-1 was performed in two pieces with primers 5′-CCCCCACCGGTAATGGCACCTGGTCCCGCACCA-3′ (oGQ 2038) introducing the 5′ AgeI site and 5′-GCGGTCTGCATTCTTGTCTG-3′ (oGQ 2056) and primers 5′-CGAATGGAACTCCGAGAACG-3′ (oGQ 2063) and 5′-CCCCTCGAGTCAGCGGCCGCCGGCCCAAATTCCGTCAG-CATC-3′ (oGQ 2068) removing the STOP and introducing 3′ NotI, a STOP, and an XhoI restriction site. Both fragments were combined by triple ligation with an overlapping intrinsic BamH1 site and cloning between AgeI–XhoI sites of L4440 vector. The complete elks-1 fragment was subcloned between AgeI–XhoI sites of pGADT7 and pGBKT7 for yeast two-hybrid analysis.

Cells of 700 μl AH109 overnight yeast culture were resuspended in 100 μl competence-inducing One-Step buffer (0.2 M lithium acetate, 40%

PEG 4000, and 100 mM DTT). About 2 µg of potential interaction partner plasmids were added and incubated at RT for 15 min and then heat shocked at 45°C for 30 s, and the suspension was plated with glass beads onto selection plates. Plates were incubated at 30°C for 2–3 d. For spotting, colonies were diluted to an OD600 of 0.2 in 100 µl. 5 µl was spotted onto minimal plates (−Leu −Trp) as control and selection plates (−Leu −Trp −His) to test for interaction.

Electrophysiology
Electrophysiological methods were performed as previously described (Richmond, 2009). In brief, animals were immobilized with Histoacryl blue glue. The ventral medial body wall muscles were exposed by a lateral cuticle incision made with a glass needle. Body wall muscle recordings were performed in the whole-cell voltage-clamp configuration (holding potential, −60 mV) using an EPC-10 patch-clamp amplifier digitized at 1 kHz. Evoked responses were elicited either by a loose patch electrode placed on the nerve cord anterior to the recorded muscle (electrical stimulation) or by applying a brief blue light pulse to retinal-treated strains expressing the cholinergic neuron ChR2 (ChR2 H134R) $zxIs6$. The 5 mM extracellular Ca^{2+} solution consisted of 150 mM NaCl, 5 mM KCl, 5 mM $CaCl_2$, 4 mM $MgCl_2$, 10 mM glucose, 5 mM sucrose, and 15 mM Hepes, pH 7.3 (~340 mOsm). The patch pipette was filled with 120 mM KCl, 20 mM KOH, 4 mM $MgCl_2$, 5 mM N-tris(hydroxymethyl) methyl-2-aminoethane-sulfonic acid, 0.25 mM $CaCl_2$, 4 mM Na_2ATP, 36 mM sucrose, and 5 mM EGTA, pH 7.2 (~315 mOsm). Data were acquired with Pulse software (HEKA). Subsequent analysis and graphing were performed using PulseFit (HEKA), Mini Analysis (Synaptosoft, Inc.), and Igor Pro (WaveMetrics).

Statistics
Data in Fig. 2, Fig. 4, Fig. 7, Fig. 8, and Fig. S3 are displayed as means with error bars indicating SEMs. Statistical analysis was performed with Prism (Prism version 5.04 for Windows; GraphPad Software). Significance is given as p-values or asterisks after Mann–Whitney tests, two-tailed Student's t test, or one-way analysis of variance with Dunnett's post test (*, $P < 0.05$; **, $P < 0.01$; ***, $P < 0.001$) for samples in which Gaussian distribution was given or assumed. Kruskal–Wallis test with Dunn's post test between selected pairs was applied for datasets that did not pass the normality test or for which normal distribution could not be assumed.

Online supplemental material
Fig. S1 shows 3D reconstructions of elongated AZ DP from neuron–neuron synapses from tomography and serial thin sections. Fig. S2 shows the gene and protein domain organizations of $syd-2$ and $elks-1$ as well as the position of the mutations and deletions used, and protein levels in the respective $syd-2$ mutants were analyzed by Western blot. Fig. S3 shows the pattern of AZ SV clusters marked by a synaptobrevin-GFP (SNB-1–GFP) fusion protein in cholinergic and GABAergic motoneurons of the different $syd-2$ mutants. Fig. S4 shows the sensitivity of the different $syd-2$ mutants to the drugs aldicarb and levamisole. Fig. S5 show a schematic representation of how the length of the presynaptic AZ DP is controlled by the activity of SYD-2 through the recruitment of ELKS-1. Online supplemental material is available at http://www.jcb.org/cgi/content/full/jcb.201302022/DC1.

References

Asperti, C., V. Astro, A. Totaro, S. Paris, and I. de Curtis. 2009. Liprin-alpha1 promotes cell spreading on the extracellular matrix by affecting the distribution of activated integrins. J. Cell Sci. 122:3225–3232. http://dx.doi.org/10.1242/jcs.054155

Brenner, S. 1974. The genetics of Caenorhabditis elegans. Genetics. 77:71–94.

Dai, Y., H. Taru, S.L. Deken, B. Grill, B. Ackley, M.L. Nonet, and Y. Jin. 2006. SYD-2 Liprin-alpha organizes presynaptic AZ formation through ELKS. Nat. Neurosci. 9:1479–1487. http://dx.doi.org/10.1038/nn1808

de Bono, M., and A.V. Maricq. 2005. Neuronal substrates of complex behaviors in C. elegans. Annu. Rev. Neurosci. 28:451–501. http://dx.doi.org/10.1146/annurev.neuro.27.070203.144259

Deken, S.L., R. Vincent, G. Hadwiger, Q. Liu, Z.W. Wang, and M.L. Nonet. 2005. Redundant localization mechanisms of RIM and ELKS in Caenorhabditis elegans. J. Neurosci. 25:5975–5983. http://dx.doi.org/10.1523/JNEUROSCI.0804-05.2005

Dresbach, T., B. Qualmann, M.M. Kessels, C.C. Garner, and E.D. Gundelfinger. 2001. The presynaptic cytomatrix of brain synapses. Cell. Mol. Life Sci. 58:94–116. http://dx.doi.org/10.1007/PL00000781

Eimer, S., A. Gottschalk, M. Hengartner, H.R. Horvitz, J. Richmond, W.R. Schafer, and J.L. Bessereau. 2007. Regulation of nicotinic receptor trafficking by the transmembrane Golgi protein UNC-50. EMBO J. 26:4313–4323. http://dx.doi.org/10.1038/sj.emboj.7601858

Feeney, C.J., S. Karunanithi, J. Pearce, and H.L. Atwood. 1998. Motor nerve terminals on abdominal muscles in larval flesh flies, Sarcophaga bullata: comparisons with Drosophila. J. Comp. Neurol. 402:197–209. http://dx.doi.org/10.1002/(SICI)1096-9861(19981214)402:2<197::AID-CNE5>3.0.CO;2-Q

Fiala, J.C. 2005. Reconstruct: a free editor for serial section microscopy. J. Microsc. 218:52–61. http://dx.doi.org/10.1111/j.1365-2818.2005.01466.x

Fouquet, W., D. Owald, C. Wichmann, S. Mertel, H. Depner, M. Dyba, S. Hallermann, R.J. Kittel, S. Eimer, and S.J. Sigrist. 2009. Maturation of active zone assembly by Drosophila Bruchpilot. J. Cell Biol. 186:129–145.

Goodman, M.B. 2006. Mechanosensation. WormBook The C. elegans Research Community, editor. http://dx.doi.org/10.1895/wormbook.1.62.1.

Hallam, S.J., and Y. Jin. 1998. lin-14 regulates the timing of synaptic remodelling in Caenorhabditis elegans. Nature. 395:78–82. http://dx.doi.org/10.1038/25757

Hallam, S.J., A. Goncharov, J. McEwen, R. Baran, and Y. Jin. 2002. SYD-1, a presynaptic protein with PDZ, C2 and rhoGAP-like domains, specifies axon identity in C. elegans. Nat. Neurosci. 5:1137–1146. http://dx.doi.org/10.1038/nn959

Harlow, M.L., D. Ress, A. Stoschek, R.M. Marshall, and U.J. McMahan. 2001. The architecture of active zone material at the frog's neuromuscular junction. Nature. 409:479–484. http://dx.doi.org/10.1038/35054000

Kaufmann, N., J. DeProto, R. Ranjan, H. Wan, and D. Van Vactor. 2002. Drosophila liprin-alpha and the receptor phosphatase Dlar control synapse morphogenesis. Neuron. 34:27–38. http://dx.doi.org/10.1016/S0896-6273(02)00643-8

Kittel, R.J., C. Wichmann, T.M. Rasse, W. Fouquet, M. Schmidt, A. Schmid, D.A. Wagh, C. Pawlu, R.R. Kellner, K.I. Willig, et al. 2006. Bruchpilot promotes active zone assembly, Ca2+ channel clustering, and vesicle release. Science. 312:1051–1054. http://dx.doi.org/10.1126/science.1126308

Ko, J., M. Na, S. Kim, J.R. Lee, and E. Kim. 2003. Interaction of the ERC family of RIM-binding proteins with the liprin-alpha family of multidomain proteins. J. Biol. Chem. 278:42377–42385. http://dx.doi.org/10.1074/jbc.M307561200

Kremer, J.R., D.N. Mastronarde, and J.R. McIntosh. 1996. Computer visualization of three-dimensional image data using IMOD. J. Struct. Biol. 116:71–76. http://dx.doi.org/10.1006/jsbi.1996.0013

Lawrence, A., J.C. Bouwer, G. Perkins, and M.H. Ellisman. 2006. Transform-based backprojection for volume reconstruction of large format electron microscope tilt series. J. Struct. Biol. 154:144–167. http://dx.doi.org/10.1016/j.jsb.2005.12.012

Liewald, J.F., M. Brauner, G.J. Stephens, M. Bouhours, C. Schultheis, M. Zhen, and A. Gottschalk. 2008. Optogenetic analysis of synaptic function. Nat. Methods. 5:895–902. http://dx.doi.org/10.1038/nmeth.1252

Liu, Q., G. Hollopeter, and E.M. Jorgensen. 2009. Graded synaptic transmission at the *Caenorhabditis elegans* neuromuscular junction. *Proc. Natl. Acad. Sci. USA*. 106:10823–10828. http://dx.doi.org/10.1073/pnas.0903570106

Nieratschker, V., A. Schubert, M. Jauch, N. Bock, D. Bucher, S. Dippacher, G. Krohne, E. Asan, S. Buchner, and E. Buchner. 2009. Bruchpilot in ribbon-like axonal agglomerates, behavioral defects, and early death in SRPK79D kinase mutants of *Drosophila*. *PLoS Genet*. 5:e1000700. http://dx.doi.org/10.1371/journal.pgen.1000700

Ohtsuka, T., E. Takao-Rikitsu, E. Inoue, M. Inoue, M. Takeuchi, K. Matsubara, M. Deguchi-Tawarada, K. Satoh, K. Morimoto, H. Nakanishi, and Y. Takai. 2002. Cast: a novel protein of the cytomatrix at the active zone of synapses that forms a ternary complex with RIM1 and munc13-1. *J. Cell Biol*. 158:577–590. http://dx.doi.org/10.1083/jcb.200202083

Patel, M.R., and K. Shen. 2009. RSY-1 is a local inhibitor of presynaptic assembly in *C. elegans*. *Science*. 323:1500–1503. http://dx.doi.org/10.1126/science.1169025

Patel, M.R., E.K. Lehrman, V.Y. Poon, J.G. Crump, M. Zhen, C.I. Bargmann, and K. Shen. 2006. Hierarchical assembly of presynaptic components in defined *C. elegans* synapses. *Nat. Neurosci*. 9:1488–1498. http://dx.doi.org/10.1038/nn1806

Phillips, G.R., J.K. Huang, Y. Wang, H. Tanaka, L. Shapiro, W. Zhang, W.S. Shan, K. Arndt, M. Frank, R.E. Gordon, et al. 2001. The presynaptic particle web: ultrastructure, composition, dissolution, and reconstitution. *Neuron*. 32:63–77. http://dx.doi.org/10.1016/S0896-6273(01)00450-0

Prokop, A., and I.A. Meinertzhagen. 2006. Development and structure of synaptic contacts in *Drosophila*. *Semin. Cell Dev. Biol*. 17:20–30. http://dx.doi.org/10.1016/j.semcdb.2005.11.010

Regus-Leidig, H., and J.H. Brandstätter. 2012. Structure and function of a complex sensory synapse. *Acta Physiol. (Oxf.)*. 204:479–486. http://dx.doi.org/10.1111/j.1748-1716.2011.02355.x

Reynolds, E.S. 1963. The use of lead citrate at high pH as an electron-opaque stain in electron microscopy. *J. Cell Biol*. 17:208–212. http://dx.doi.org/10.1083/jcb.17.1.208

Richmond, J. 2005. Synaptic function. *WormBook*. The *C. elegans* Research Community, editor. http://dx.doi.org/10.1895/wormbook.1.69.1.

Richmond, J. 2009. Dissecting and recording from the *C. Elegans* neuromuscular junction. *J. Vis. Exp*. 24:e1165. http://dx.doi.org/10.3791/1165.

Rostaing, P., R.M. Weimer, E.M. Jorgensen, A. Triller, and J.L. Bessereau. 2004. Preservation of immunoreactivity and fine structure of adult *C. elegans* tissues using high-pressure freezing. *J. Histochem. Cytochem*. 52:1–12. http://dx.doi.org/10.1177/002215540405200101

Schoch, S., and E.D. Gundelfinger. 2006. Molecular organization of the presynaptic active zone. *Cell Tissue Res*. 326:379–391. http://dx.doi.org/10.1007/s00441-006-0244-y

Schoch, S., P.E. Castillo, T. Jo, K. Mukherjee, M. Geppert, Y. Wang, F. Schmitz, R.C. Malenka, and T.C. Südhof. 2002. RIM1alpha forms a protein scaffold for regulating neurotransmitter release at the active zone. *Nature*. 415:321–326. http://dx.doi.org/10.1038/415321a

Serra-Pagès, C., Q.G. Medley, M. Tang, A. Hart, and M. Streuli. 1998. Liprins, a family of LAR transmembrane protein-tyrosine phosphatase-interacting proteins. *J. Biol. Chem*. 273:15611–15620. http://dx.doi.org/10.1074/jbc.273.25.15611

Shin, H., M. Wyszynski, K.H. Huh, J.G. Valtschanoff, J.R. Lee, J. Ko, M. Streuli, R.J. Weinberg, M. Sheng, and E. Kim. 2003. Association of the kinesin motor KIF1A with the multimodular protein liprin-alpha. *J. Biol. Chem*. 278:11393–11401. http://dx.doi.org/10.1074/jbc.M211874200

Sieburth, D., Q. Ch'ng, M. Dybbs, M. Tavazoie, S. Kennedy, D. Wang, D. Dupuy, J.F. Rual, D.E. Hill, M. Vidal, et al. 2005. Systematic analysis of genes required for synapse structure and function. *Nature*. 436:510–517. http://dx.doi.org/10.1038/nature03809

Spangler, S.A., and C.C. Hoogenraad. 2007. Liprin-alpha proteins: scaffold molecules for synapse maturation. *Biochem. Soc. Trans*. 35:1278–1282. http://dx.doi.org/10.1042/BST0351278

Stigloher, C., H. Zhan, M. Zhen, J. Richmond, and J.L. Bessereau. 2011. The presynaptic dense projection of the *Caenorhabditis elegans* cholinergic neuromuscular junction localizes synaptic vesicles at the active zone through SYD-2/liprin and UNC-10/RIM-dependent interactions. *J. Neurosci*. 31:4388–4396. http://dx.doi.org/10.1523/JNEUROSCI.6164-10.2011

Sudhof, T.C. 2004. The synaptic vesicle cycle. *Annu. Rev. Neurosci*. 27:509–547. http://dx.doi.org/10.1146/annurev.neuro.26.041002.131412

Takao-Rikitsu, E., S. Mochida, E. Inoue, M. Deguchi-Tawarada, M. Inoue, T. Ohtsuka, and Y. Takai. 2004. Physical and functional interaction of the active zone proteins, CAST, RIM1, and Bassoon, in neurotransmitter release. *J. Cell Biol*. 164:301–311. http://dx.doi.org/10.1083/jcb.200307101

Tao-Cheng, J.H., J. Du, and C.J. McBain. 2000. Snap-25 is polarized to axons and abundant along the axolemma: an immunogold study of intact neurons. *J. Neurocytol*. 29:67–77. http://dx.doi.org/10.1023/A:1007168231323

Taru, H., and Y. Jin. 2011. The Liprin homology domain is essential for the homomeric interaction of SYD-2/Liprin-α protein in presynaptic assembly. *J. Neurosci*. 31:16261–16268. http://dx.doi.org/10.1523/JNEUROSCI.0002-11.2011

van Roessel, P., D.A. Elliott, I.M. Robinson, A. Prokop, and A.H. Brand. 2004. Independent regulation of synaptic size and activity by the anaphase-promoting complex. *Cell*. 119:707–718. http://dx.doi.org/10.1016/j.cell.2004.11.028

Wagh, D.A., T.M. Rasse, E. Asan, A. Hofbauer, I. Schwenkert, H. Dürrbeck, S. Buchner, M.C. Dabauvalle, M. Schmidt, G. Qin, et al. 2006. Bruchpilot, a protein with homology to ELKS/CAST, is required for structural integrity and function of synaptic active zones in *Drosophila*. *Neuron*. 49:833–844. http://dx.doi.org/10.1016/j.neuron.2006.02.008

Wagner, O.I., A. Esposito, B. Köhler, C.W. Chen, C.P. Shen, G.H. Wu, E. Butkevich, S. Mandalapu, D. Wenzel, F.S. Wouters, and D.R. Klopfenstein. 2009. Synaptic scaffolding protein SYD-2 clusters and activates kinesin-3 UNC-104 in *C. elegans*. *Proc. Natl. Acad. Sci. USA*. 106:19605–19610. http://dx.doi.org/10.1073/pnas.0902949106

Wang, Y., M. Okamoto, F. Schmitz, K. Hofmann, and T.C. Südhof. 1997. Rim is a putative Rab3 effector in regulating synaptic-vesicle fusion. *Nature*. 388:593–598. http://dx.doi.org/10.1038/41580

Wang, Y., X. Liu, T. Biederer, and T.C. Südhof. 2002. A family of RIM-binding proteins regulated by alternative splicing: Implications for the genesis of synaptic active zones. *Proc. Natl. Acad. Sci. USA*. 99:14464–14469. http://dx.doi.org/10.1073/pnas.182532999

Weimer, R.M., E.O. Gracheva, O. Meyrignac, K.G. Miller, J.E. Richmond, and J.L. Bessereau. 2006. UNC-13 and UNC-10/rim localize synaptic vesicles to specific membrane domains. *J. Neurosci*. 26:8040–8047. http://dx.doi.org/10.1523/JNEUROSCI.2350-06.2006

Wojcik, S.M., and N. Brose. 2007. Regulation of membrane fusion in synaptic excitation-secretion coupling: speed and accuracy matter. *Neuron*. 55:11–24. http://dx.doi.org/10.1016/j.neuron.2007.06.013

Wyszynski, M., E. Kim, A.W. Dunah, M. Passafaro, J.G. Valtschanoff, C. Serra-Pagès, M. Streuli, R.J. Weinberg, and M. Sheng. 2002. Interaction between GRIP and liprin-alpha/SYD2 is required for AMPA receptor targeting. *Neuron*. 34:39–52. http://dx.doi.org/10.1016/S0896-6273(02)00640-2

Yeh, E., T. Kawano, R.M. Weimer, J.L. Bessereau, and M. Zhen. 2005. Identification of genes involved in synaptogenesis using a fluorescent active zone marker in *Caenorhabditis elegans*. *J. Neurosci*. 25:3833–3841. http://dx.doi.org/10.1523/JNEUROSCI.4978-04.2005

Zanazzi, G., and G. Matthews. 2009. The molecular architecture of ribbon presynaptic terminals. *Mol. Neurobiol*. 39:130–148. http://dx.doi.org/10.1007/s12035-009-8058-z

Zhai, R.G., and H.J. Bellen. 2004. The architecture of the active zone in the presynaptic nerve terminal. *Physiology (Bethesda)*. 19:262–270. http://dx.doi.org/10.1152/physiol.00014.2004

Zhen, M., and Y. Jin. 1999. The liprin protein SYD-2 regulates the differentiation of presynaptic termini in *C. elegans*. *Nature*. 401:371–375.